

We are IntechOpen, the world's leading publisher of Open Access books Built by scientists, for scientists

4,800

Open access books available

122,000

International authors and editors

135M

Downloads

Our authors are among the

154

Countries delivered to

TOP 1%

most cited scientists

12.2%

Contributors from top 500 universities



WEB OF SCIENCE™

Selection of our books indexed in the Book Citation Index
in Web of Science™ Core Collection (BKCI)

Interested in publishing with us?
Contact book.department@intechopen.com

Numbers displayed above are based on latest data collected.
For more information visit www.intechopen.com



Growth and Characterization of Doped CaF₂ Crystals

Irina Nicoara and Marius Stef
*West University of Timisoara, Timisoara,
Romania*

1. Introduction

The alkaline-earth fluorides crystallize in the cubic structure and constitute an important class of relatively simple ionic crystals whose optical and lattice-dynamical properties have theoretical and experimental interest. The CaF₂ crystals have been used for long time in many optical components due to its exceptional transparency in the UV as well as in the IR spectral domain. CaF₂, SrF₂ and BaF₂ have been among the first solid-state laser hosts and they were lased at the beginning of the 1960s doped with RE³⁺ ions; these rare-earth doped crystals, however, have been abandoned as laser systems during a long time. The reason resides in the charge compensation which is required to maintain the electrical neutrality of crystals. This process gives rise to a rich multisite structure including so-called isolated centers and more or less complex centers [Petit et al., 2008], which leads to broad absorption and emission bands comparable with those of glasses. Rare earth doped CaF₂ recently have a new interest firstly because it was found that clustering of ions in these materials could be favorable to produce some infrared laser emission. Yb³⁺ -doped CaF₂ has been proved in recent years to be one of the most attractive Yb³⁺ laser materials for different reasons. It is also proved that the proportions of the different luminescent centers vary with the considered RE³⁺ ion and with the nature of the substituted divalent cation. It is expected, indeed that the transition strengths associated with various centers are different; for example, the transition strengths associated with tetragonal centers will be greater than those of the trigonal ones. At high dopant concentrations (about 1 at%) which become interesting for the laser application, the ions generally aggregate and form more or less complex centers that in turn can weaken the emission transitions. Such a detrimental pairing effect can be decreased and some improvement can be obtained by co-doping the crystals with charge compensating buffer ions, such as monovalent ions or non-optically active rare-earth trivalent ions. For example, after Na⁺ ions were introduced as charge compensators the IR emission intensity of the Yb³⁺-doped CaF₂ crystal was enhanced several times [Su et al., 2007].

Taking into account the interesting properties of CaF₂ crystals doped with various impurities, in this work we describe our investigations about the optical properties of Pb²⁺, Yb³⁺ doped CaF₂ crystals, as well as the influence of Na⁺ ions on the formation of various charge compensating defects.

2. Crystal growth

Crystallization process is essentially a phenomenon of periodic arrangement of the constituent ions of a given material obtaining a crystalline state. There are many methods of crystal growth. Controlled solidification in a crucible of a molten material is one of the most used method. First used by Bridgman [Bridgman, 1925], improved by Stockbarger [Stockbarger, 1949] this technique is used successfully (about 40% of production of artificial crystals) because it is a simple technology and does not require complicated control systems. In the design of vertical Bridgman-type technique (VB) it is important to predict the thermal profiles in the growing crystal. The position and shape of the solidification interface and the axial and radial thermal gradients are of particular interest in controlling the growth process. The relatively high axial temperature gradient necessary in order to obtain crystals with large diameters ($\Phi > 20\text{mm}$) cannot be obtained by means of a single heating element; two or more independently controlled heaters are necessary. The temperature gradient is directly dependent on the "isolated" zone between the hot and cold zones [Fu&Wilcox, 1980; Mikkelsen, 1980]. In order to obtain crystals with melting temperature higher than 1300°C , graphite, molybdenum, silicon carbide, etc heaters must be used [Stockbarger, 1949; Gault et al., 1986; Jones et al., 1966]; the high temperature gradient necessary at the crystallization interface is obtained either by supplementary heaters [Stockbarger, 1949; Jones et al., 1966], by thermal screen translation or by using two heaters with a moving temperature gradient and a stationary crucible [Gault et al., 1986]. Taking into account the analysis of the heat transfer in VB technique [Chang&Wilcox, 1974; Fu&Wilcox, 1980; Naumann, 1982; Jasinski et al., 1983], we designed [D.Nicoara, 1975; D. Nicoara et al., 1985a; D. Nicoara et al., 1985b; I. Nicoara et al., 1987; D. Nicoara&I. Nicoara, 1988] several types of graphite heaters whose characteristics would satisfy the growth conditions to obtain crystals with melting point up to 2000°C . In this paragraph we will focus on the growth particularities in order to obtain pure and various concentrations of PbF_2 , YbF_3 -doped and NaF-codoped CaF_2 crystals using Bridgman technique [D. Nicoara&I. Nicoara, 1988; Nicoara et al., 2008a, 2008b; Pruna et al., 2009; Paraschiva et al., 2010]

2.1 Shaped graphite heaters

The general view of the crystal growth set-up is shown in figure 1a [D.Nicoara 1975]. Figure 1b illustrates the longitudinal section of three types of heaters and the temperature distribution along them. The model contains an adiabatic zone and a booster heater zone that can be used to increase the thermal gradient near the solidification interface. Built of graphite (see fig 7), the heater produces an almost constant temperature zone (the B-C hot zone) necessary to melt the charge and a high gradient temperature zone (D-E). The C zone (the booster heater) ~ 20 mm long in the case of type I heater is designed as a meander-type resistance with wall thickness of 1.5 mm, by means of which an overheating is obtained in the lower level of the upper zone. The D zone is inserted for the improvement of heat transfer upwards the upper part of the heater, the E zone ~ 10 mm long, which appears like a wall thickening (up to 5 mm), has the role of an "isolated" zone and allows to reach a high temperature gradient. The F zone -the cold zone - is used as the lower cooling chamber. The wall thickness of this zone increases from 1.5 mm to 4 mm in the lower part. The wall thickness of the II type heater in the B zone decreases from 3mm to 2mm; the C zone is ~ 15

mm long with wall thickness of 1.5 mm. The III type heater produces a relatively flat temperature profile in the hot zone B-C. The wall thickness decreases gradually from 3 mm in the upper part of the B zone to 1.5 mm in the C-D zone, then increases to 4mm in the lower part of the F zone. Curve I represents the temperature distribution in I type heater and the curve I_a is the temperature recorded during the growth of a 30 mm diameter CaF₂ crystal. Comparing these two distributions one can see that the furnace parameters were well chosen, the axial temperature distribution remaining approximately the same. In order to avoid thermal loss, the graphite heater is surrounded by a set of concentric screens made of molybdenum, graphite, and stainless steel.

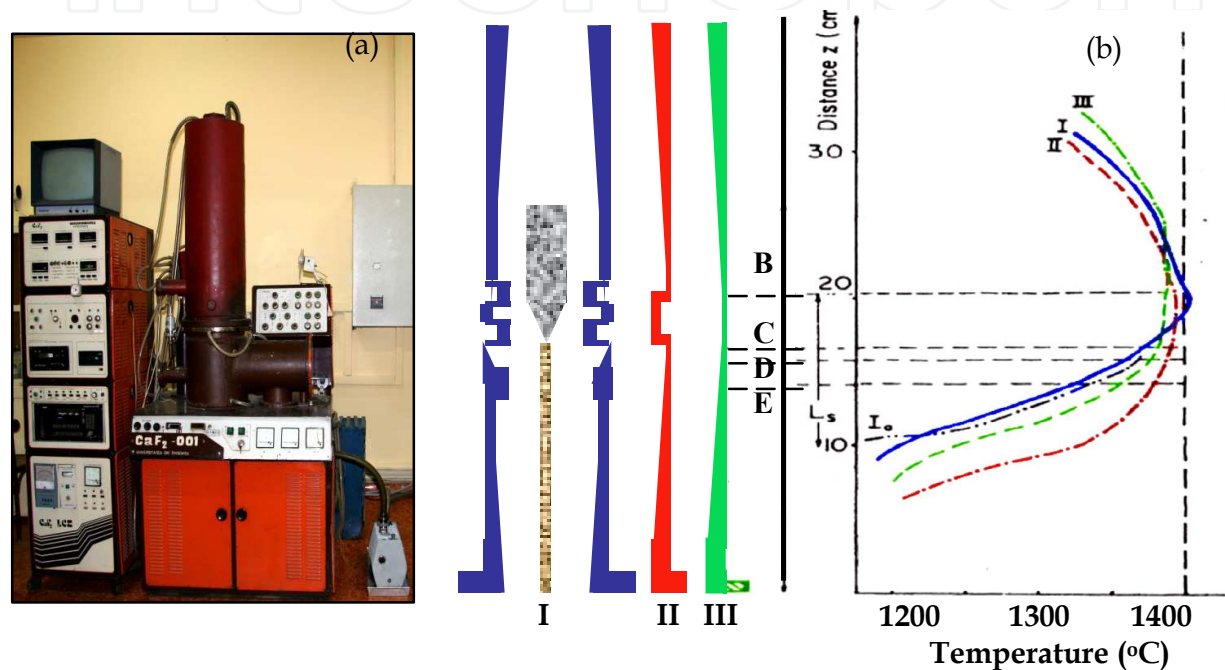


Fig. 1. (a) The crystal growth set-up; (b) Longitudinal sections of three types of heaters and temperature distribution along them, [D. Nicoara, 1975; D. Nicoara et al., 1985a,b].



Fig. 2. (a) Calcium fluoride crystals; (b) multiple type crucible; (c) crucible with seed.

In order to obtain crystals, with diameter up to 10 mm, the C zone can be eliminated, the necessary temperature gradient (7-10⁰ C/cm) can be obtained only by the heater wall thickness adjustments, like III type heater. For crystals with diameter less than 20 mm, type II and III heaters could be employed. Using these types of heaters fluoride single crystals

with diameter of up to 50 mm and 150 mm in length were obtained (fig. 2a). With a multiple type crucible [D. Nicoara et al., 1985a; 1985b] several up to 12 mm diameter crystals can be obtained during a single growth process (fig. 2b). Oriented crystal can be grown using a seed (Fig. 2 c) [D. Nicoara et al., 1983].

The thermal stresses can be reduced by gradual cooling rate to room temperature. After the crystal pulling is finished, the crucible is raised in the B-C zone and by using an automatic system the power supply is gradually lowered.

From our experiments it can be concluded that the use of these types of heaters in the VB technique in order to obtain high quality fluoride crystals is advantageous because the same heater can be used for about hundred growth processes, the growth conditions being reproducible and easy to control.

2.2 Growth of PbF_2 -doped CaF_2 crystals

PbF_2 -doped CaF_2 crystals were grown in our crystal research laboratory using vertical Bridgman method. Suprapure grade (Merck) calcium fluoride and PbF_2 were used as the starting materials. It is known [Stockbarger, 1949; Yonezawa et al., 2002] that Pb^{2+} ions hardly remain in fluoride crystals if the usual VB technique is used for the growth of CaF_2 crystals. In order to obtain PbF_2 -doped CaF_2 crystals the following procedure was used. First, pure, oxygen-free CaF_2 crystals were grown using the usual growth conditions, namely adding to the starting material an amount of 4 wt% PbF_2 as oxygen scavenger [Stockbarger, 1949]. The obtained CaF_2 crystals do not contain any undesired amount of lead ions or other impurities, as results from the optical absorption spectrum; then the PbF_2 -doped crystals were grown from the crushed pure fluoride crystals doped with the desired amount of PbF_2 . To prevent the evaporation of the PbF_2 , a thin floating graphite lid was put on the charge in a sealed graphite crucible. Transparent colorless crystals of about 10 mm in diameter over 6–7 cm long were obtained in spectral pure graphite crucible in vacuum ($\sim 10^{-1}$ Pa) using a shaped graphite furnace [D. Nicoara&I. Nicoara, 1988]. The pulling rate was 4 mm/h. The crystals were cooled to room temperature using an established procedure. The as-grown single crystals are shown in Fig. 3.

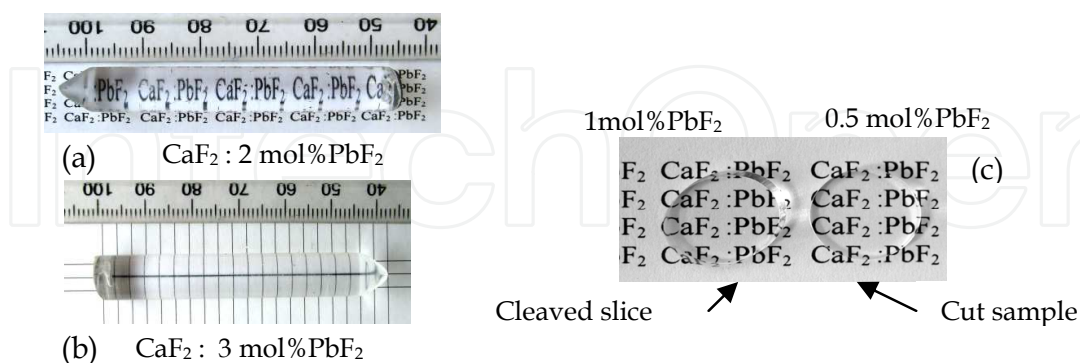


Fig. 3. As-grown x mol% PbF_2 -doped CaF_2 crystals: (a) $x = 2$; (b) $x = 3$; (c) cleaved slice of 1 mol% PbF_2 doped CaF_2 crystal and cut sample of 0.5 mol% PbF_2 doped CaF_2 crystal.

CaF_2 crystallizes in cubic structure with a typical fluorite lattice. In order to understand the optical properties and the dopant distribution in CaF_2 crystals it is better to see this structure as consisting of a simple cubic lattice of fluorine ions in which every other body center position is occupied by a Ca^{2+} ion. When various ions, such as alkaline metals, rare-earths or

heavy metal ions, like Pb²⁺ are introduced into the lattice they usually occupy Ca²⁺ sites. If the introduced impurity ions have other valence than the Ca²⁺ ion, the valence mismatch is compensated in a variety of ways: by vacancy formation, by interstitial fluorine ion, etc. The Pb²⁺ ion has the same valence as Ca²⁺ but with a larger geometric size (0.143 nm) than the Ca²⁺ ion (0.126 nm), and for high dopant concentrations this will lead to distortion of the crystal lattice; this is the reason why the crystals doped with more than 3 mol%PbF₂ reveal structural defects, like blocks with different crystallographic orientations (Figure 4).

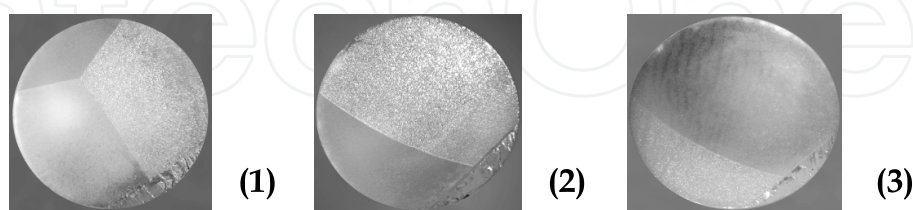


Fig. 4. Misoriented high PbF₂ concentration sample; (1) the 2mm thick sample was cut from the bottom of the crystal, (2) after 4mm only two blocks remain and (3) after other 2 mm a single oriented crystal appears.

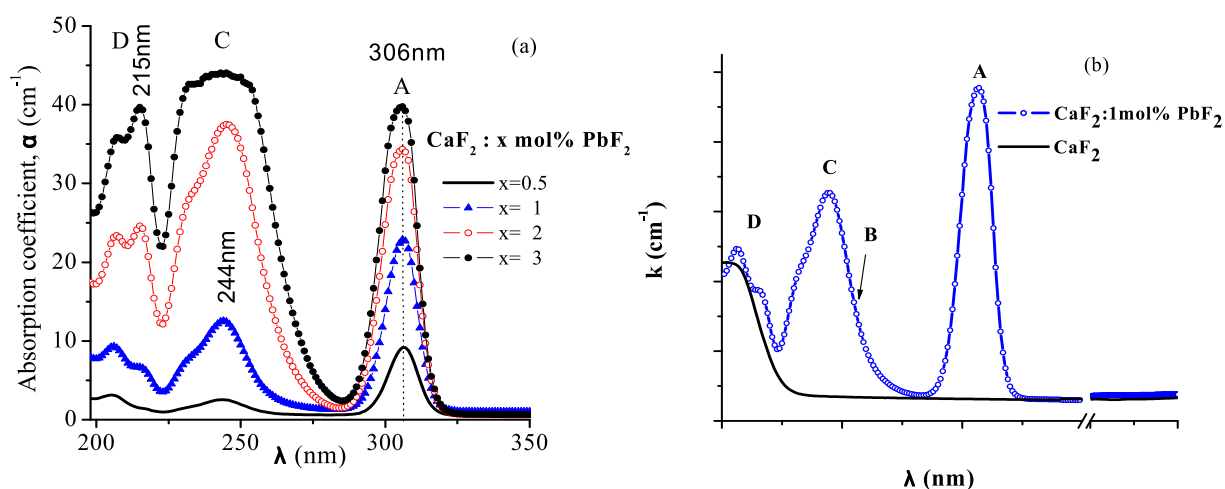


Fig. 5. (a) Room temperature absorption spectra of PbF₂ doped CaF₂ crystals; (b) absorption spectra of pure and 1 mol%PbF₂-doped CaF₂ crystals.

The presence of impurity ions in CaF₂ lattice with the *ns*² ground state configuration (like Pb²⁺ ions) induces absorption bands both in vacuum ultraviolet (VUV) and in UV domain [Jacobs, 1991]. Four characteristic bands are located in UV domain, denoted by A, B, C, and D [Jacobs, 1991]. The absorption spectra of various concentrations CaF₂:PbF₂ samples reveal the four characteristic absorption bands of Pb²⁺ ions (Fig. 5). As Pb²⁺ -ions concentration increases, the shape of the C and D absorption bands modifies due to the overlap of many new bands that appear as a result of the energy levels splitting, only the A band conserves his sharp shape.

2.3 Rare-earth ions-doped CaF₂ crystals

Rare-earth (RE) ions-doped CaF₂ crystals are used as laser active media due to the well-known good optical, mechanical and thermal properties of the CaF₂ host and due to the

broad band transitions of the various RE ions. The optical properties of the Yb^{3+} ions in the CaF_2 host are well known and the luminescence properties have been intensively studied due the strong near-IR emission that can be easily pumped with laser diodes. It is known that several of RE ions, such as Sm, Eu, Ho, Tm and Yb, can be stabilized in the divalent state in alkaline earth halide lattices, besides the trivalent state, with which can coexist. The spectroscopic properties of the Yb^{2+} ions have been less investigated, mainly only for its intense and broad yellow-green (540–560 nm) luminescence [Feofilov, 1956; Kaplyanskii&Feofilov, 1962; Kaplyanskii et al., 1976]. When YbF_3 is dissolved in CaF_2 , normally the ytterbium ions are in the trivalent state, but it is known that a certain fraction of any of RE^{3+} ions can be reduced to divalent state by various methods.

The change of the valence can be attained by exposing the crystals to ionizing radiation, baking them in a suitable atmosphere [Kirton&McLaughlan, 1967; Kaczmarek et al., 2005] or by electrolytic reduction [Fong, 1964]. The observed emission is weak for the crystals containing Yb^{2+} ions obtained using one of these methods. There are a few reported results [Feofilov, 1956; Kaplyanskii&Feofilov, 1962; Kaplyanskii&Smolyanskii 1976] about the properties of the Yb^{2+} ions, with high concentration in the as-grown crystals. The intense broad yellow-green luminescence has been obtained only for low temperature. Near-UV luminescence at room temperature has not been reported. This was one of the reason why we studied the spectroscopic properties of YbF_3 -doped CaF_2 crystals with high divalent ytterbium content in the as-grown crystals. In order to obtain high Yb^{3+} - Yb^{2+} conversion in the as grown crystals, we have developed a special growth procedure.

Rare-earth ions -doped and PbF_2 -codoped CaF_2 crystals were grown using vertical Bridgman method [Nicoara et al., 2006a, 2006b, 2008a, 2008b, 2008c; Pruna et al., 2009; Paraschiva, 2010]. As starting materials suprapure grade calcium fluoride, YbF_3 , ErF_3 and PbF_2 have been used. The $\text{Yb}:\text{CaF}_2$ and $\text{Er}:\text{CaF}_2$ crystals were obtained by adding YbF_3 and ErF_3 to the melts in molar concentrations varying between 0.07 and 2 mol%. First, pure CaF_2 crystals were grown using the standard growth conditions. In all cases, 0.4wt% PbF_2 was used as oxygen scavenger. Fig. 5a shows the time dependence of the power (in arbitrary units) and temperature in the furnace in order to determine the growth conditions.

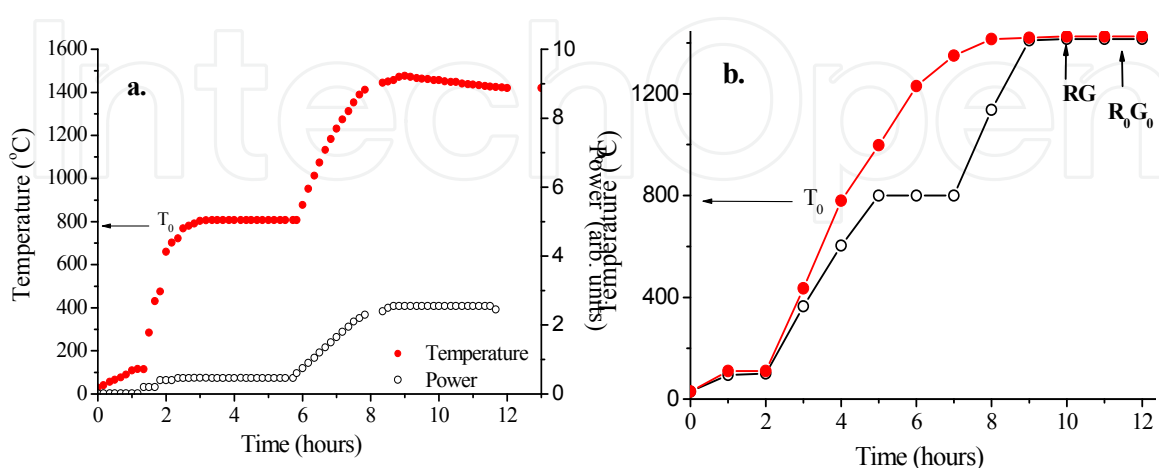


Fig. 6. (a) Time dependence of the temperature in the furnace (the position P in figure 7) against the power (in arbitrary units); (b) various growth conditions.

If the crystal growth process is not correctly established (for example, the T_0 temperature is not reached and then keep the raw material for 3 h at a temperature lower than T_0), the obtained crystals may contain some amount of undesired lead ions. This is why we study the influence of the Pb^{2+} ions on the optical properties of the YbF_3 -doped CaF_2 crystals [Nicoara et al., 2006b; 2008b]. The growth procedure started to run after the whole furnace chamber was vacuumed to 10^{-1} Pa; the temperature was kept at $1000^\circ C$ for 3 h to remove water from the raw materials and then 3 h at $T_0=800^\circ C$ to eliminate the PbO obtained after the reaction $CaO+PbF_2 \rightarrow CaF_2+PbO$.

Pure CaF_2 crystals were grown using the conditions shown in the Fig. 6b, alternative 1. The obtained CaF_2 crystals do not contain any undesired lead ions amount, as seen in the optical absorption spectrum (Fig. 5. the inset).

The YbF_3 (or ErF_3)-doped CaF_2 crystals were grown from crushed pure CaF_2 crystals obtained using a correct growth process. No oxygen scavenger has been added in order to obtain the doped crystals; in this case the alternative 2 shown in figure 6b was used.

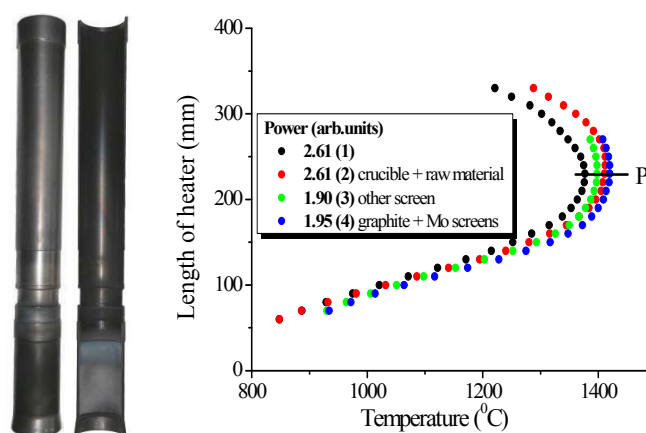


Fig. 7. Axial temperature distribution in the furnace for various powers and growth conditions: (1) without crucible and charge, (2) with crucible and charge, supplementary screen, (3) other positions of the screen, (4) double screen: graphite and molybdenum.

In order to obtain Pb^{2+} codoped crystals, 1 mol% PbF_2 was added in the starting mixture in melt. To prevent the evaporation of the PbF_2 , a thin graphite lid was put on the charge in the sealed crucible. In order to obtain Pb^{2+} codoped $YbF_3 : CaF_2$ crystals, alternative 2 (fig. 6b) was used. The crystal growth begins by lowering the crucible in the temperature distribution in the furnace shown in Fig. 7. For alternative 1 the growth process starts to run at position R_0G_0 (the Fig. 6b) and for alternative 2 at RG.

Transparent colorless crystals (CaF_2 , $CaF_2 : YbF_3$, $CaF_2 : YbF_3 + PbF_2$; $CaF_2 : YbF_3 + NaF$; $CaF_2 : PbF_2$) of about 10mm in diameter over 6–7 cm long were obtained. The crystals were cooled to room temperature using an established procedure. The as-grown single crystals are shown in Fig. 8. The ErF_3 doped crystals are transparent pink color.

The optical absorption spectra (190–1090 nm) reveal the characteristic UV absorption bands of the Yb^{2+} ions with more than 10 times higher absorption coefficient than the one of the Yb^{3+} ions (see Fig. 9). We assigned the high Yb^{2+} ions content in the as-grown crystals to the reducing conditions during the growth process due to the presence of the graphite components of the growth set-up and the lack of the oxygen scavenger during the growth of the doped crystals.

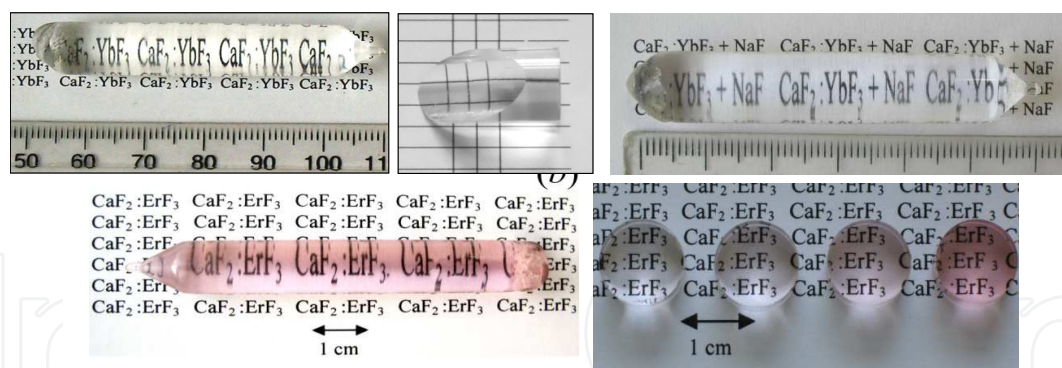


Fig. 8. As-grown crystals: (a) CaF_2 : 0.17 mol% YbF_3 ; (b) CaF_2 : 0.7 mol% YbF_3 +2.5 mol% NaF ; (c) CaF_2 :2mol% ErF_3 ; (d) CaF_2 : x mol% ErF_3 , x= 0.69, 0.8, 1.1, 5.

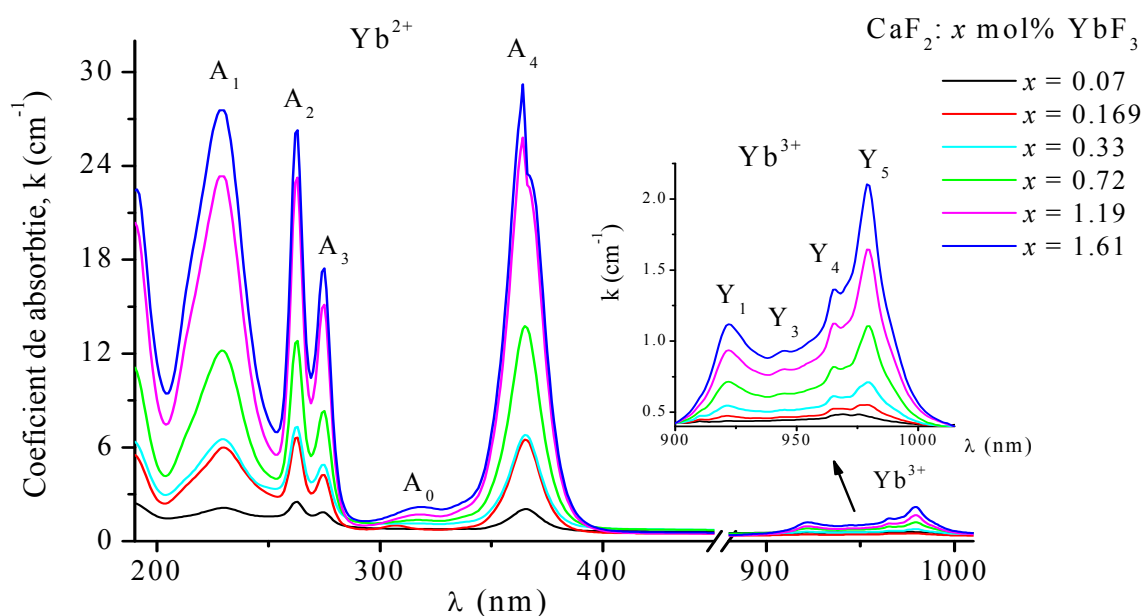


Fig. 9. Absorption spectra of YbF_3 doped CaF_2 crystals.

In order to obtain YbF_3 -doped CaF_2 and NaF codoped crystals the following procedure was used. First, pure, oxygen-free CaF_2 crystals were grown using the usual growth procedure, namely adding to the starting material an amount of 4 wt% PbF_2 as an oxygen scavenger. The obtained CaF_2 crystals do not contain any undesired lead ions amount or other impurities, as results from the optical absorption spectrum; these crystals were then crushed and the powder was doped with the desired amount of YbF_3 and NaF codopant. To prevent the evaporation of NaF , a thin floating graphite lid was put on the charge in a sealed graphite crucible.

3. Characterization

Taking into account that these crystals are used as optical materials for various purposes it is important to know how the impurities influence the optical properties of the crystals. Various structural defects appear, from the so-called isolated centers to more or less complex centers. In order to study the structural defects in crystals we used various methods as are described below.

3.1 Dislocations distribution in crystals

The quality of the crystals was studied by examining the dislocations distribution using the chemical etching method. For this purpose the fresh cleavage surface (111) of the crystal were subjected to etching in aqueous solution of 2N-8N HCl.

The effect of temperature and concentration of HCl aqueous solutions on the etching behavior on the cleavage surface of CaF₂ crystals was investigated [Nicoara et al., 1986]. It has been observed that the shape and the evolution of etch pits and the values of dissolution rate depend on the etching conditions. This behavior suggests that the dissolution rate along a certain direction changes with the temperature and the etchant concentrations. Taking into the ionic arrangement in the (111) plan of the CaF₂, the experimental observations [Sangval&Arora, 1978] and the theoretical considerations [Benson & Dempsey, 1962] on the repulsive energy between the two fluoride ions, we suppose that the activation energy depends on the crystallographic directions on the (111) surface and on the etching parameters. These explain the shape of the etch pits. Various etch pits shapes were also observed in doped calcium fluoride crystals.

The formation, multiplication and high mobility of the dislocations in ionic crystals lead not only to high densities of individual dislocations, but also cause arrangements of dislocations into well-developed grain sub-boundaries, which are stable and nearly immobile in contrast to individual dislocations (fig 10). Sub-boundaries cannot be easily removed by annealing. Some sub-boundaries appear at the beginning of the growth process.

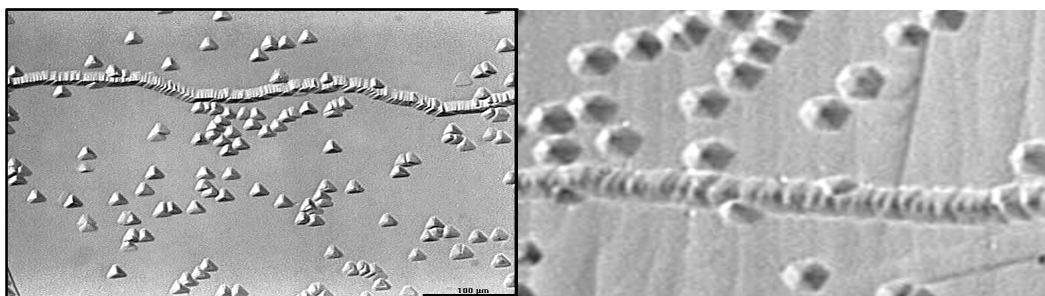


Fig. 10. Individual etch pits and grain sub-boundaries.

An interesting feature is shown in the cross-section of the crystals that are grown in multiple crucibles: the dislocation density is greater in that part of the crystal which is oriented towards the axis support of the crucible [Nicoara et al., 1987]. This fact is explained by the existence of an inadequate radial temperature gradient, the crucible being asymmetrically placed in the thermal field of the furnace, one of its parts near the hot wall. This disadvantage is eliminated by attaching a reflective molybdenum cylindrical screen to the axis, which ensures uniform thermal field for the crucible assembly.

The dislocation density along the sample and for a given cross-section in radial direction was examined. The density of the etch pits and sub-boundaries is quite low and fairly uniform through the sample for crystals with diameter up to 12 mm which were grown in a I type heater with a rate of 6 mm/h and temperature gradient of 70 C/ cm. The dislocation density is about 10³-10⁴ dis/cm². For higher pulling rate the dislocation density increases [Nicoara et al., 1986; 1987].

The influence of the various dopant and dopant concentration on the dislocations density and etch pits morphologies were studied. The dislocation density and the etch pits shape observed in various crystals are summarized in figure 11 and table 1 and 2.

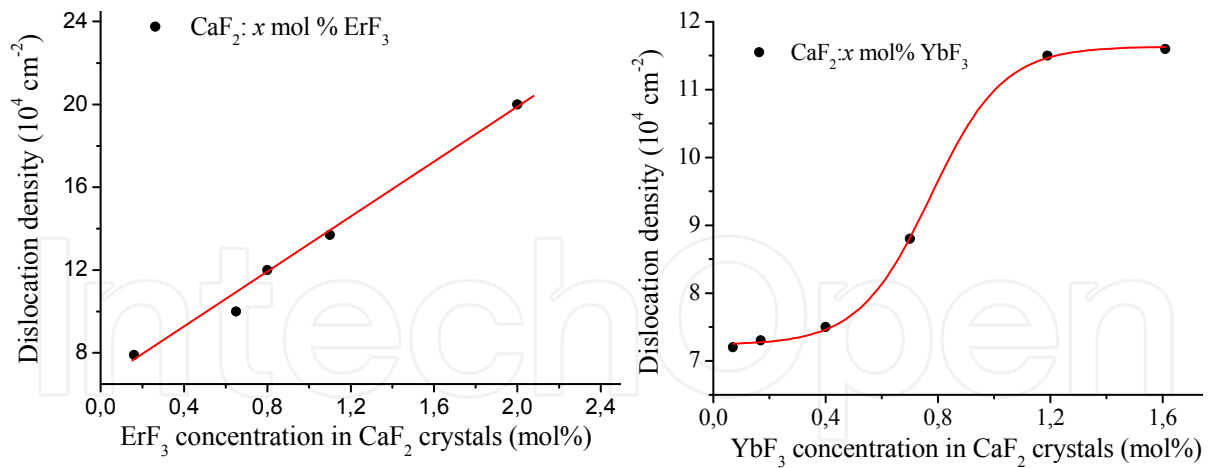


Fig. 11. Dislocation density vs dopant concentration.


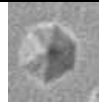


$\text{CaF}_2 : x \text{ mol}\% \text{ErF}_3$	$x=0.17$	$x=0.69$	$x=0.8$	$x=1.1$
Etch pit shape				
Dislocation density	$7.9 \cdot 10^4$	$10 \cdot 10^4$	$11.9 \cdot 10^4$	$13.7 \cdot 10^4$

Table 1. Dislocation density (dis/cm²) and etch pit shape in ErF_3 doped CaF_2 crystals.

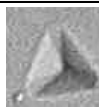


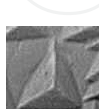


Crystal	Etch pit shape	Dislocation density (dis/cm ²)	Etch pit dimensions (μm)
CaF_2		$5.5 \cdot 10^4$	18; 4.6; 15.7; 3.7; 16.4; 3.7;
CaF_2 : 1 mol% PbF_2		$6.0 \cdot 10^4$	38.9; 33.8; 40.9
CaF_2 : 2 mol% PbF_2		$6.6 \cdot 10^4$	5.1; 15.3; 5.0 12.3; 4.5; 16.2
CaF_2 : 0.169 mol% YbF_3		$7.3 \cdot 10^4$	47.6; 37.9; 42;
CaF_2 : 0.7 mol% YbF_3		$8.8 \cdot 10^4$	22; 22.7; 22.3;
CaF_2 :1.2 mol% YbF_3 + 2.5 mol% NaF		$12.3 \cdot 10^4$	12; 3; 11.5; 3; 11.3; 3;

Table 2. Etch pit shape and dislocation density in doped CaF_2 crystals.

3.2 Dopant distribution along the crystals

The homogeneous distribution of the dopant in laser crystals is important because this affects the efficiency of the laser.

The effective segregation coefficient (k_{eff}) at a given growth rate is defined by

$$k_{eff} = C_S / C_L^0, \quad (1)$$

where C_S is the dopant concentration at the bottom of the as-grown crystal and C_L^0 is the dopant concentration in the initial melt. The value of C_S can be measured by various methods, or estimated from optical absorption measurements [Kuwano, 1982; Sun et al., 2005].

The effective segregation coefficient determination of the Er³⁺, Yb³⁺, Yb²⁺ and Pb²⁺ ions in CaF₂ host by optical absorption method is based on the following two laws.

(a) According to the Beer-Lambert law the absorption coefficient is proportional to the sample concentration (C), $a = aC$ where a is the absorption coefficient for unit ion concentration and unit light path length; a may be recognized as constant for the investigated ions concentration [Kuwano, 1982; Sun et al., 2005]. The various ions concentration can be estimated from the measured optical density,

$$O.D. = \log(I_0 / I) \quad (2)$$

where I_0 is the light intensity incident on the sample, I is the transmitted light intensity.

Taking into account the relation

$$I = I_0 \exp(-a \cdot d) \quad (3)$$

where a is the absorption coefficient and d is the sample thickness, the dopant concentration of a slice can be estimated using the relation [Kuwano, 1982]:

$$C = \frac{a}{a} = \frac{O.D. \cdot 2.30258}{a \cdot d} \quad (4)$$

(b) The dopant concentration (along the growth axis) at the distance z from the origin of the crystal can be obtained by using the classical relation [Hurle, 1993]:

$$C_S(z) = C_L^0 k_{eff} [1 - g(z)]^{k_{eff} - 1} \quad (5)$$

where $g(z)$ is the crystallized fraction of the melt given by $g(z) = Vt/L = z/L$, V is the crystal growth rate, t is the growth time and L is the crystal length, so Vt is the grown crystal length, z , at the moment t . The more the k_{eff} differs from unity, the larger is the concentration gradient in the crystal.

Taking into account the Beer-Lambert law, the dopant distribution along the crystal length can be estimated using the optical absorption method. In order to determine the effective segregation coefficient, we cut the crystal into i slices with the same thickness (Fig. 12) and calculated the absorption coefficient for a particular absorption peak, from the optical absorption spectrum of every slices ($a(z)$). Using the relations (4) and (5), the following expression is obtained in order to determine the effective segregation coefficient:

$$\lg \alpha(z) = (k_{\text{eff}} - 1) \lg(1 - z/L) + \lg(ak_{\text{eff}}C_L^0) \quad (6)$$

The effective segregation coefficient can be calculated from the slope $m = k_{\text{eff}} - 1$, of the fitting line of $\lg \alpha(z)$ versus $\lg(1-z/L)$. This was the method used to calculate the segregation coefficient.

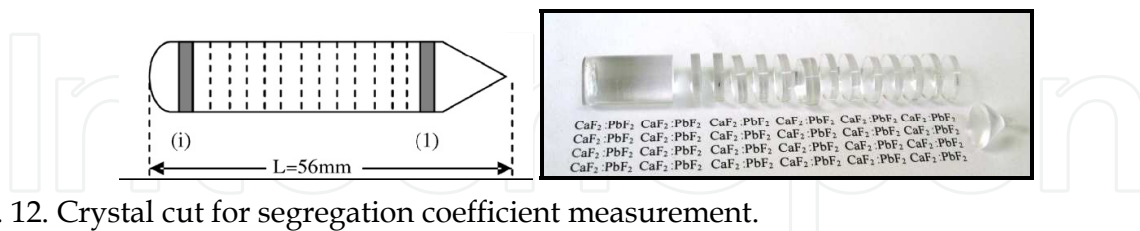


Fig. 12. Crystal cut for segregation coefficient measurement.

Segregation coefficient of Yb^{3+} and Yb^{2+} ions

Room-temperature optical absorption spectra were recorded using a Shimadzu 1650PC spectrophotometer. The absorption coefficient increases as the YbF_3 concentration in the CaF_2 host increases. Fig. 13 shows the influence of the YbF_3 concentration on the absorption coefficient of the peaks at 979 nm and 365 nm.

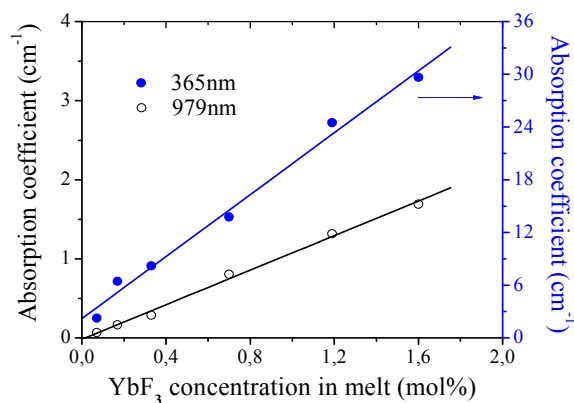


Fig. 13. Dependence of the absorption coefficient of 979 nm and 365 nm on the initial YbF_3 concentration in the melt.

The variation of Yb^{2+} and Yb^{3+} ions' concentration distribution along the as-grown crystals has been studied only for two concentrations, namely with YbF_3 added to the melt in molar concentrations equal to 0.7 mol% and 1.6 mol%.

The absorption coefficient $\alpha(z)$ of every slice was calculated from the absorption spectra for two characteristic absorption bands: 979 nm for Yb^{3+} ions and 365 nm for Yb^{2+} ions [Nicoara et al., 2008a; Nicoara et al., 2008b]. Fig. 14a shows the Yb^{3+} ions' concentration (characterized by the absorption coefficient, α) distribution along the crystals. For both investigated crystals the absorption coefficient of the slides is almost constant along the crystals; this means that the trivalent Yb ions are distributed homogeneously along the crystals. The slope of the fitting line of the Yb^{3+} ions concentration distribution along the crystals, namely of $\lg \alpha(z)$ vs. $\lg(1-z/L)$ (Fig. 14b), have been used to calculate the segregation coefficient of Yb^{3+} ions in $\text{YbF}_3:\text{CaF}_2$ crystals. The obtained values of the segregation coefficient are close to the unity for both investigated crystals: $k \approx 1.00$ for the $\text{CaF}_2:1.61 \text{ mol\% YbF}_3$ sample and $k \approx 0.98$ for the $\text{CaF}_2:0.72 \text{ mol\% YbF}_3$ sample; this indicates a rather homogeneous distribution of Yb^{3+} ions in $\text{YbF}_3:\text{CaF}_2$ crystals [Nicoara et al., 2008b]. These values are in good agreement with those reported, for example $k \approx 1.07$ for $\text{CaF}_2:1.96 \text{ at\% YbF}_3$ [Su et al., 2005].

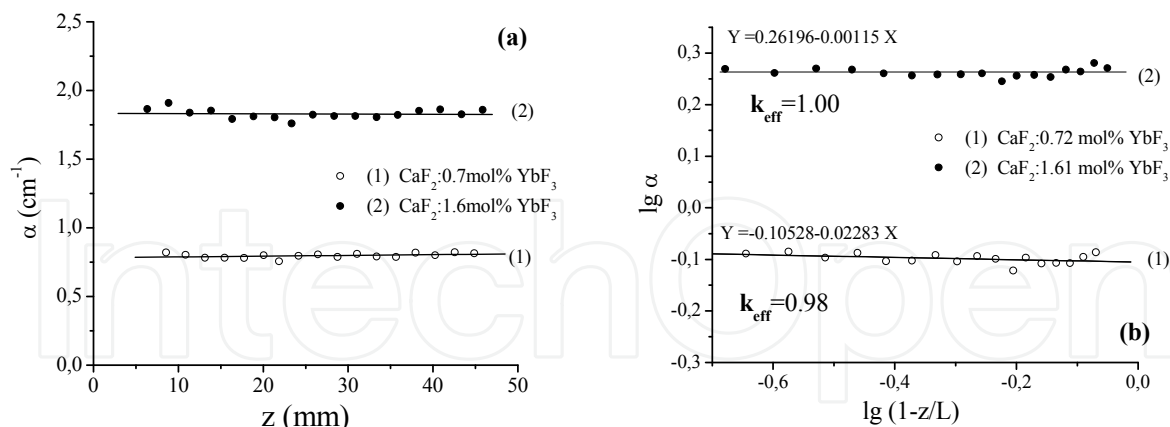


Fig. 14. (a) Yb³⁺ ions distribution along the crystal; (b) fitting lines of $\lg \alpha$ vs $\lg (1-g)$.

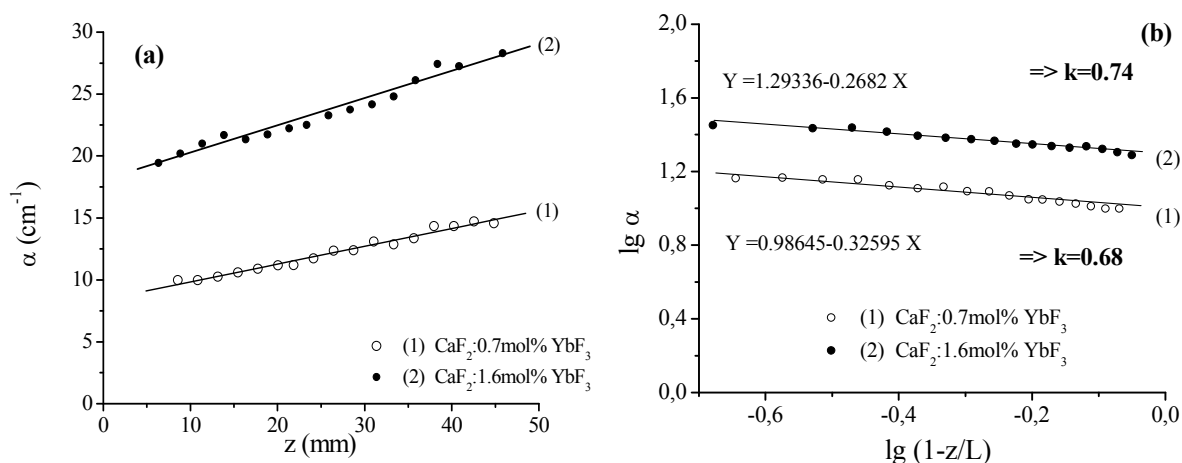


Fig. 15. (a) Yb²⁺ ions distribution along the crystal; (b) fitting line of $\lg \alpha$ vs $\lg (1-g)$.

Fig. 15a shows the Yb²⁺ ions concentration (characterized by the absorption coefficient, α) distribution along the crystals. The absorption coefficient increases along the crystals, and as the concentration of YbF₃ in the initial melt increases the absorption coefficient, α , increases too. The fitting lines of $\lg a(z)$ vs. $\lg (1-g)$ for the two studied Yb:CaF₂ crystals are shown in Fig. 6b. The segregation coefficient is less than unity for both crystals: $k \approx 0.68$ for the CaF₂:1.6mol% YbF₃ sample and $k \approx 0.74$ for the CaF₂:0.72mol% YbF₃ sample. The more k differs from unity, the larger the dopant concentration gradient along the crystal is and hence, no homogeneous distribution of Yb²⁺ ions in YbF₃: CaF₂ crystals can be obtained.

Segregation coefficient of Er³⁺

The segregation coefficient of the Er³⁺ ion in CaF₂ host was determined for two ErF₃ concentrations: 0.8mol% ErF₃ and 2 mol%ErF₃ using the method described above.

The absorption coefficient $a(z)_i$ of every slice i was calculated from the absorption spectra for the following absorption peaks: 406nm, 968nm and 979nm. The dopant distribution along the crystals shows some oscillations of the Er³⁺-ions concentration. These types of oscillations have also been observed for other crystals grown by Bridgman technique; this behavior was not explained yet [Barat, 1995; Mitric et al., 2006]. The strongest oscillatory

behavior of the dopant distribution along the crystal has been observed for the CaF_2 : 2mol% ErF_3 sample.

The obtained values of effective the segregation coefficient are: $k_{\text{eff}} = 1.01$ -0.99 for CaF_2 : 0.8mol% ErF_3 sample and 1.03-1.04 for CaF_2 : 2mol% ErF_3 crystal [Munteanu et al., 2010]. As the concentration of the ErF_3 in the initial melt increases the effective segregation coefficient, k_{eff} , increases too; the dependence of the effective segregation coefficient on the dopant concentration was also observed in other host [Lifante et al., 1999; Barraldi et al., 2005]. Because the effective segregation coefficient is almost equal with unity, the Er^{3+} ions distribution in CaF_2 crystals is approximately uniform along the crystal and from this point of view, ErF_3 - doped CaF_2 crystals could be a good laser material.

Segregation coefficient of Pb^{2+}

Figure 16 shows the Pb^{2+} ions distribution (characterized by the absorption coefficient) along the four investigated crystals, with various PbF_2 concentrations in the initial melt. The dopant distribution along the crystals shows some oscillations of the Pb^{2+} ions concentration. For CaF_2 : 2 mol% PbF_2 sample the dopant distribution along the crystal has the strongest oscillatory behavior. The calculated effective segregation coefficient for the studied samples is: 0.85 for CaF_2 : 0.5 mol% PbF_2 crystal, 0.925 for CaF_2 : 1mol% PbF_2 crystal, 1.002 for CaF_2 :2 mol% PbF_2 crystal and 1.15 for CaF_2 :3 mol% PbF_2 crystal.

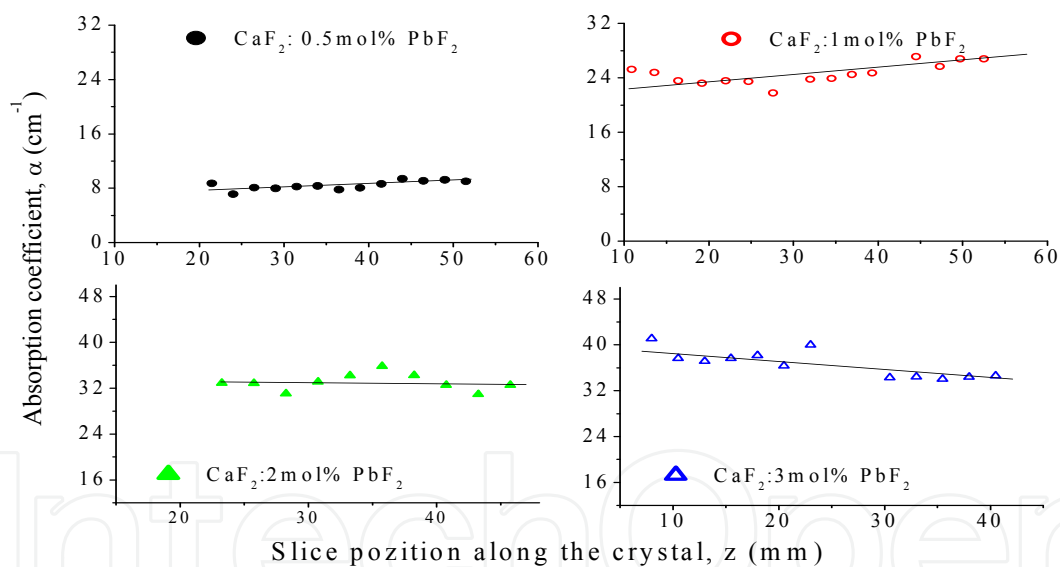


Fig. 16. Variation of the absorption coefficient along the PbF_2 doped CaF_2 crystals

As the concentration of the Pb^{2+} ions in the initial melt increases, the effective segregation coefficient increases, too [Paraschiva et al., 2010]. Dependence of the segregation coefficient of different ions in the CaF_2 host on the dopant concentration is shown in fig. 17.

3.3 Dielectric relaxation

Information on impurity-defect aggregates can be obtained from spectroscopic studies and dielectric relaxation technique. The optical absorption provides information about the nature and site symmetry of the defects. Trivalent RE ions in CaF_2 tend to form pairs of adjacent ions, for charge compensation, even at low RE concentrations. The extra positive

charge is usually compensated by interstitial F⁻ ions. Besides the tetragonal (C_{4v}) symmetry of the predominant dipolar complex, many other simple or cluster configurations appear. The resultant dipolar complexes can reorient by “jumps” of one of the charges to other lattice sites. In order to use the laser properties of the crystals it is necessary to study the influence of the various type of defects introduced by various impurities, such as the RE activator ions or other ions on the properties of the crystals. Information on impurity-defect aggregates can be obtained from spectroscopic and dielectric relaxation techniques, the last being sensitive to aggregates with a dipole moment which can reorient through migration of the anions. Temperature and frequency dependence of the complex dielectric constant give information about the relaxation processes and permits the determination of the activation energy and the reciprocal frequency factor, τ_0 , of the relaxation time, τ , and the number of dipoles that contribute to the relaxation process. [Fontanella& Andeen, 1976; Andean et al., 1977; Fontanella&Tracy, 1980; Andeen et al., 1979; Andeen et al., 1981].

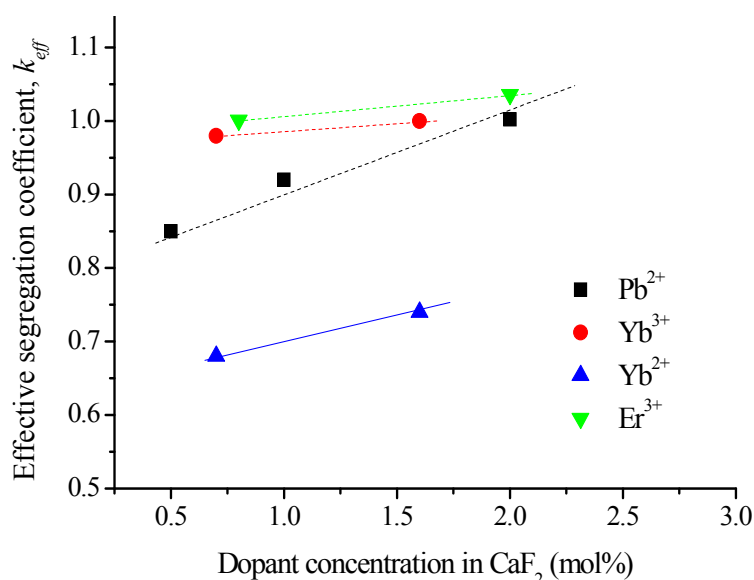


Fig. 17. Dependence of the k_{off} on the dopant concentration for Pb²⁺, Yb²⁺, Yb³⁺ și Er³⁺ ions.

The impurity-defects in CaF₂ crystals doped with various ions-Er³⁺, Yb³⁺, Pb²⁺ and Na⁺ - were studied using the dielectric relaxation method [Nicoara et al., 2006; Nicoara et al., 2006b; Nicoara et al., 2008; Pruna et al., 2009].

Capacitance (C) and dielectric loss ($D=tan\delta$) measurements were performed on the samples using a RLC Meter type ZM2355, NF Corporation, Japan over the temperature range of 150–320 K at seven audio-frequencies. The real part of the complex dielectric constant, ϵ_1 , was calculated from the measured capacitance C. The imaginary part of the complex dielectric constant, ϵ_2 was then calculated from $D=\epsilon_2 / \epsilon_1$. Linear heating rates of 2 K/min were employed from liquid nitrogen to room temperature. The dielectric properties have been measured on the 10 mm diameter and 0.6 mm thick disks using an Ag (Leitsilber) contacts. The measurements have been performed on as the (111) cleavage plane as on perpendicular to growth direction cut samples. Using this method we obtained information about the influence of dopant concentration on the formation of various charge compensating defects in doped CaF₂ crystals.

After doping some dipolar complex appear which can reorient (relax) by “jumps” of one of the charges to other lattice sites. Such dipoles are usually characterized by a relaxation time, τ given by

$$\tau = \tau_0 \exp(E/kT) \quad (7)$$

In order to determine the activation energy for reorientation, E , and the reciprocal frequency factor τ_0 , the complex dielectric constant $\varepsilon(\omega, T) = \varepsilon_1(\omega, T) + i\varepsilon_2(\omega, T)$ has to be determined. The real and imaginary parts of the complex dielectric constant are given by the Debye equations. Since ε_2 has a maximum for $\omega\tau = 1$, it follows from Eq. (1) that: $\ln\omega = -(E/kT_{\max}) - \ln\tau_0$, where T_{\max} is the temperature at which ε_2 has a maximum at a given frequency and E and τ_0 can be determined from the plot of T_{\max}^{-1} vs $\ln\omega$.

Dependence of the real and the imaginary part of the complex dielectric constant of $\text{CaF}_2:0.17 \text{ mol\% ErF}_3$ sample on the temperature and on the frequency is plotted in Fig. 18.

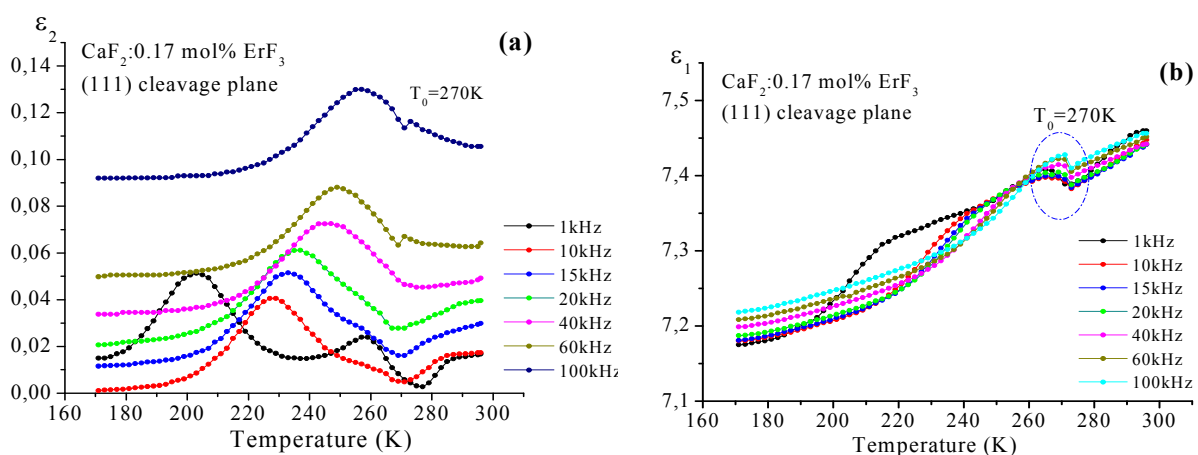


Fig. 18. Temperature and frequency dependence of (a) the imaginary part and (b) real part of the complex dielectric constant. The measurements have been made on (111) cleavage plane.

The peaks occurring at higher temperature as the frequency increases is associated to the R_I , Debye-like relaxation [Fontanella&Andeen, 1976] due to the relaxation of $\text{Er}^{3+} - \text{F}_i$ pair in which the F occupies the nearest-neighbor (NN) interstitial position with respect to the Er^{3+} ion. The R_{IV} relaxation [Fontanella&Andeen, 1976] (around 240-260 K, with activation energy $> 0.5 \text{ eV}$) increases as the concentration increases and is very clear only for Pb^{2+} -codoped samples [Nicoara et al., 2008]. The values of the relaxation parameters for the observed relaxations are shown in the Table 3.

The value of ε_1 and ε_2 increases as the rare-earth ions concentration increases; around $T_0 = 269 \text{ K}$ an anomaly of ε_1 and ε_2 behavior has been observed which can be assigned with a phase transition of the order-disorder type. The temperature dependence of the dielectric constant and loss tangent for this sample is shown in Fig. 19a. The loss tangent has a maximum at a slightly lower temperature than the ε_1 maximum and a sharp minimum at a slightly higher temperature. The temperature dependence of the reciprocal of ε_1 against $T - T_0$ is shown in Fig. 19b. We can observe that the slopes of the $\varepsilon_1^{-1}(T)$ plots are different on both sides of T_0 . These types of anomalies in the dielectric properties have been observed for some perovskite-type compounds [Smolenskii et al., 1958] and are assigned with an order-disorder type phase transition [Strukov&Levanyuk, 1998].

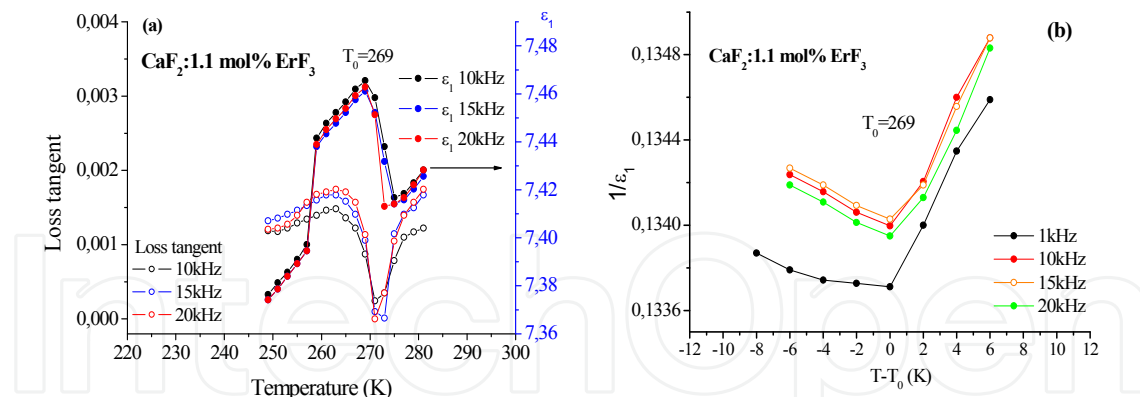


Fig. 19. (a) Temperature dependence of ϵ_1 and of the loss tangent. (b) Temperature dependence of the reciprocal dielectric constant.

The dielectric spectra of YbF₃ doped CaF₂ crystals has same behavior as described below, the obtained relaxation parameters are summarized in Table 3.

It has been observed [Doualan et al., 2010;] that the detrimental pairing effect of the RE ions [Corish et al., 1982; Petit et al., 2007; Petit et al., 2008] can be decreased by co-doping the crystals with charge compensating buffer ions, such as monovalent ions, like Na⁺ ions [Doualan et al., 2010; Su et al., 2005, 2007] or non-optically active rare-earth trivalent ions. In the case of the double doped (with Yb³⁺ and Na⁺ ions) CaF₂ crystals, the Na⁺ can work also as charge compensator for Yb³⁺ ions, entering in interstitial (or substitutional) positions near the Yb³⁺ ion and leading to C_{3v} (or C_{2v}) symmetry, sites without dipolar properties. In conclusion, codoping with Na⁺ leads to new (Na⁺-V_F) and (Yb³⁺-Na⁺) centers. These defects can be studied using the dielectric relaxation. Five YbF₃ -doped crystals were investigated with the following amount of YbF₃ added in the starting mixture in the melt: 0.07, 0.17, 0.72, 1.19 and 1.6 mol% YbF₃; six NaF co-doped YbF₃:CaF₂ crystals with different Na:Yb ratios of R=2, 4, 16, 28, 36 have been also grown.

A typical temperature and frequency dependence of the real and imaginary parts of the complex dielectric constant is plotted in Fig. 20 for CaF₂: 0.16 mol% YbF₃ + 2.5 mol % NaF sample (R=16). The value of ϵ_1 and ϵ_2 increases as the YbF₃ concentration increases. In the range of the investigated temperatures, for YbF₃ doped CaF₂ crystals there is only one maximum in the temperature dependence of ϵ_2 , at a given frequency, that corresponds to relaxation of NN (C_{4v}) dipoles [Fontanella & Andeen, 1976]. An "anomaly" of ϵ_1 and ϵ_2 behavior, like a maximum has been observed around the temperature $T_0 = 270$ -279 K for YbF₃ doped samples and 275-276 K for NaF codoped samples, depending on the sample concentration (Fig. 20 and 21a). The value of the temperature T_0 does not depend on the frequency, so is not a relaxation. This behavior is assigned to an order-disorder type phase transition.

The temperature and frequency dependence of ϵ_2 for Na⁺ ions co-doped samples, for ratio R<20 is characterized by three peaks (Fig. 20b, 21a). For all samples the peak occurring at around 195 K at 1 kHz is associated to the R₁ (NN) center relaxation. The second peak is associated to the order-disorder transition and the third peak, that appears only for Na⁺ ions codoped crystals, is associated to (Na⁺-V_F) dipoles relaxation, formed by a substitutional Na⁺ ion and a F⁻ vacancy created to maintain the electrical neutrality of the crystal [Johnson et al., 1969; Shelley & Miller, 1970].

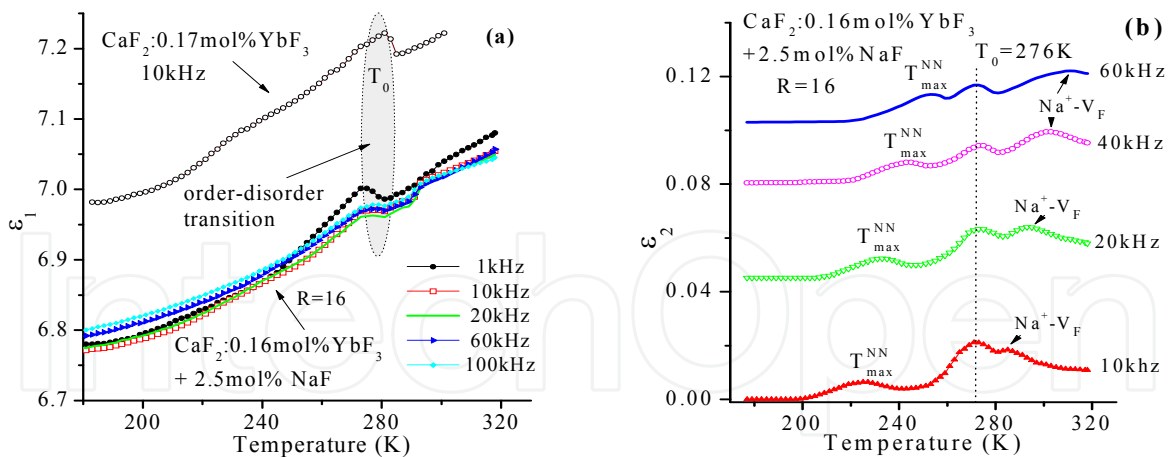


Fig. 20. Temperature and frequency dependence of (a) the real part and (b) the imaginary part of the complex dielectric constant

For heavier NaF- codoped samples, namely for ratio $R > 20$, only one relaxation is observed, associated to the $(\text{Na}^+ - \text{V}_\text{F})$ dipole (see Fig.21b). This confirms the observed suppression of the peaks of optical absorption spectra, corresponding to centers with C_{4v} (NN dipole) symmetry.

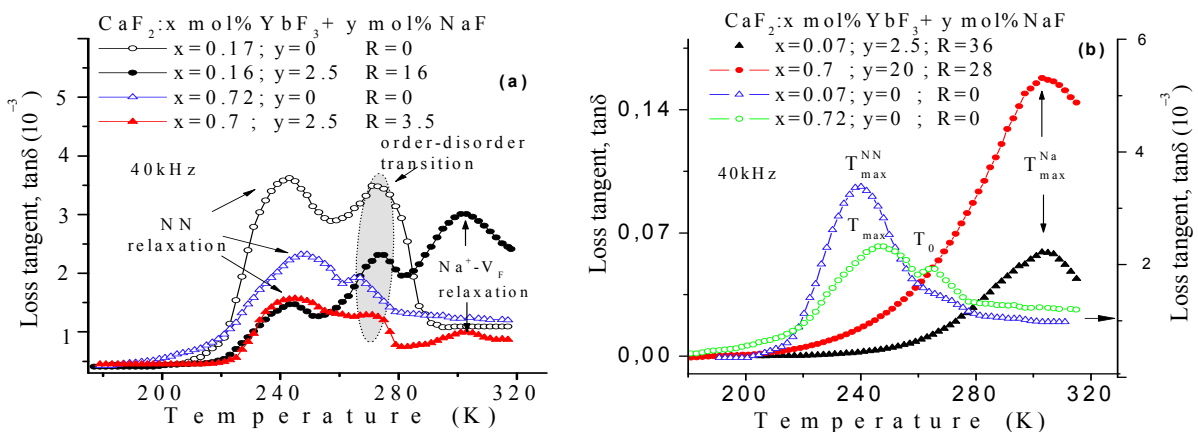


Fig. 21. Influence of Na^+ ions on the loss tangent for (a) low and (b) for high R ratios.

The number of dipoles N_D that contribute to the dielectric relaxation peak can be calculated from the dielectric spectra using the methods described in [Fontanella&Andeen, 1976; Campos&Ferreira, 1974].

Figure 22a shows the variation of the number of NN dipoles (N_{NN}) with the YbF_3 concentration for un-codoped and 2.5mol%NaF codoped samples. The number of NN dipoles that contributes to the dielectric loss peak decreases as the Yb^{3+} ions concentration increases. This effect was also observed by Fontanella [Fontanella&Andeen, 1976] for $\text{CaF}_2:\text{ErF}_3$ samples doped with concentration higher than 0.1mol%. This indicates that as the YbF_3 concentration increases the predominant dipoles are NNN and/or clusters types (that relax at lower and/or higher temperature than we have investigated), diminishing in this way the number of dipoles that contribute to the dielectric relaxation of NN (C_{4v} symmetry) type dipoles.

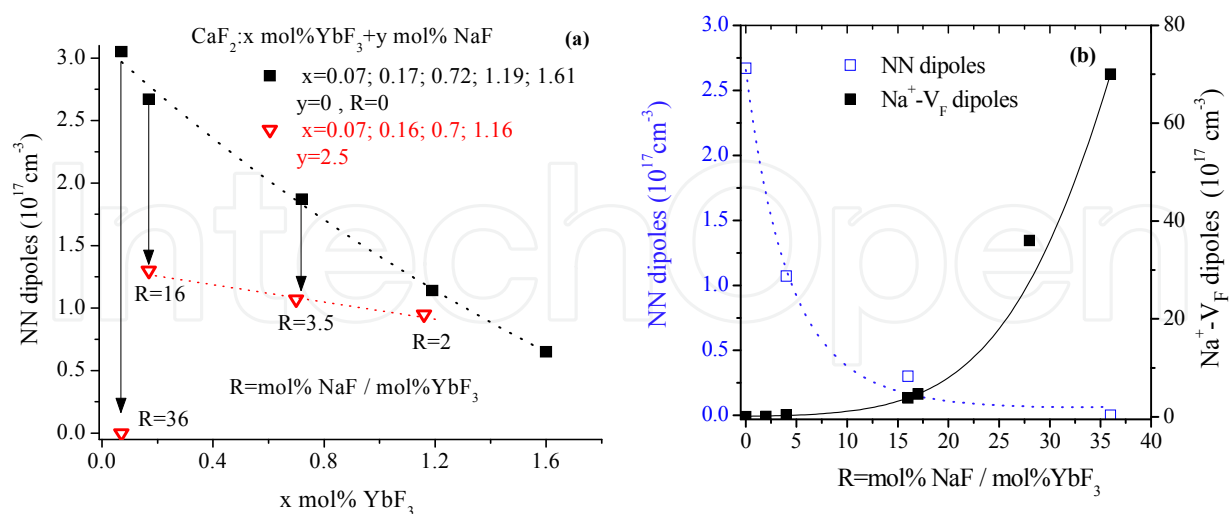


Fig. 22. (a) Influence of YbF_3 concentration and ratio R on the NN dipoles concentration for samples doped with 2.5 mol% NaF (open symbols); (b) Influence of ratio R on the NN and $\text{Na}^+ - \text{V}_F$ dipoles concentration

The Na^+ ions co-doped $\text{YbF}_3:\text{CaF}_2$ crystals reveal a decrease of the NN dipoles in comparison with the YbF_3 -doped samples, indicating that the Na^+ ions reduce the formation of NN type dipoles with C_{4v} symmetry; this is confirmed by the absorption spectra. This effect depends on the ratio $R = \text{ymol\% NaF} / \text{xmol\% YbF}_3$, as is shown in Figs. 22a,b; as the ratio R increases, the number of NN (C_{4v}) centers decreases and the number of ($\text{Na}^+ - \text{V}_F$) dipoles increases (fig. 22b); for ratio $R=28$ and 36 no NN type relaxation was detected (fig. 21b), this means a very small concentration of C_{4v} sites.

CaF ₂ :	0.17 mol% ErF ₃	0.69 mol% ErF ₃	1.1 mol% ErF ₃	0.5 mol% PbF ₂	1 mol% PbF ₂
dipole	(Er ³⁺ - F ⁻)NN	(Er ³⁺ - F ⁻) NN	(Er ³⁺ - F ⁻)NN	(Pb ²⁺ - F _{vac})	(Pb ²⁺ - F _{vac})
E(eV)	0.383	0.335	0.345	0.438	0.358
τ_0 (s)	$5.1 \cdot 10^{-14}$	$26.2 \cdot 10^{-14}$	$52 \cdot 10^{-14}$	$1 \cdot 10^{-14}$	$3 \cdot 10^{-14}$
CaF ₂ :	0.07 mol% YbF ₃	0.17 mol% YbF ₃	0.72 mol% YbF ₃	CaF: 0.17 mol% YbF ₃ + 2.5 mol% NaF	
dipole	(Yb ³⁺ - F ⁻)NN	(Yb ³⁺ - F ⁻)NN	(Yb ³⁺ - F ⁻)NN	(Yb ³⁺ - F ⁻) NN	(Na ⁺ - F _{vac})
E(eV)	0.35	0.42	0.34	0.305	0.515
τ_0 (s)	$2.1 \cdot 10^{-13}$	$0.055 \cdot 10^{-13}$	$4.4 \cdot 10^{-13}$	$2.1 \cdot 10^{-12}$	$7.45 \cdot 10^{-15}$

Table 3. Relaxation parameters.

3.4 Tailoring the charge compensating defects in YbF₃ doped CaF₂ crystals

When YbF₃ is dissolved in CaF₂, normally the Yb ions are in a trivalent state. It is also known that a certain fraction of any of RE³⁺ ions can be reduced to divalent state depending on the growth conditions. The Yb³⁺-ions usually occupy a cation substitutional position, but charge compensation is required to maintain the electrical neutrality of the system; the extra positive charge is compensated by an interstitial fluorine ion (F_i⁻). For low YbF₃ concentration (< 0.1mol%), besides the O_h cubic symmetry with no local charge compensation, the so-called isolated dipolar centers are predominant with tetragonal symmetry (C_{4v}) in which the F_i⁻ ion occupies a nearest-neighbor (NN) interstitial site and trigonal (C_{3v}) NNN site [Kirton&McLaughlan, 1967; Corish et al., 1982; Petit et al., 2007; Petit et al., 2008]. At higher Yb³⁺ ion concentrations, the dopant ions aggregate and form more or less complex clusters [Corish et al., 1982; Petit et al., 2007; Petit et al., 2008]. Such a complicated structure leads to broad optical absorption bands. The detrimental pairing effect can be decreased by co-doping the crystals with charge compensating buffer ions, such as monovalent ions [Doualan et al., 2010; Su et al., 2005, 2007] or non-optically active rare-earth trivalent ions. After Na⁺ ions were introduced as charge compensators the IR emission intensity of the YbF₃-doped CaF₂ crystal was enhanced several times [Su et al., 2005, 2007].

When a Na⁺ ion is introduced into the CaF₂ lattice, this enters substitutionally and is compensated by a fluorine vacancy (Na⁺ -V_F) [Johnson et al. 1969; Shelley&Miller, 1970; Fontanella et al., 1980]. In the case of the double doped (with Yb³⁺ and Na⁺ ions) CaF₂ crystals, the Na⁺ can work also as charge compensator for Yb³⁺ ions, entering in interstitial (or substitutional) positions near the Yb³⁺ ion and leading to C_{3v} (or C_{2v}) symmetry, sites without dipolar properties. In conclusion, codoping with Na⁺ leads to new (Na⁺ -V_F) and (Yb³⁺-Na⁺) centers.

In order to study the varieties of Yb³⁺ sites in CaF₂ host, several YbF₃ doped and NaF-codoped CaF₂ crystals with different Na:Yb ratios were grown by Bridgman method. Six NaF co-doped YbF₃:CaF₂ crystals with different Na:Yb ratios of 2, 4, 16, 28, 36 have been also grown. Room temperature absorption spectra and dielectric spectra were measured to study the effect of Na⁺ ions on the charge compensating defects formation [Pruna et al., 2009].

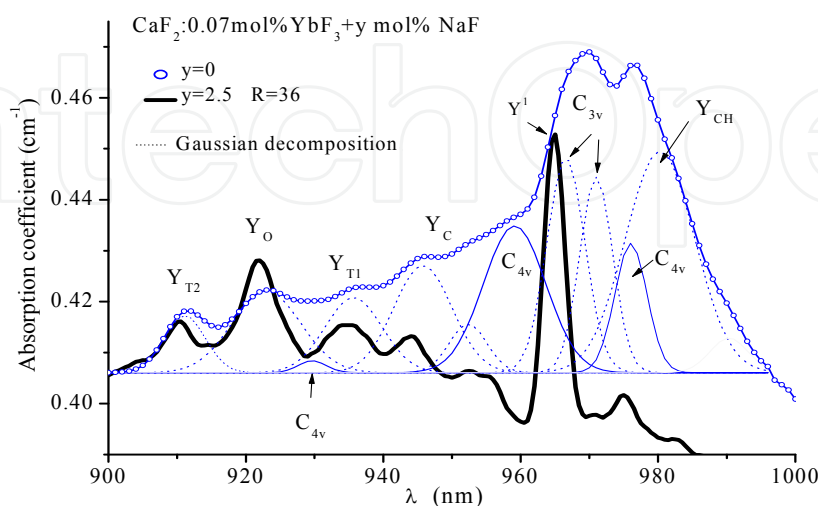


Fig. 23. Absorption spectra of (0.07mol%YbF₃+ymol%NaF):CaF₂ crystals; the decomposition by Gaussian multi-peak fits is shown for CaF₂:0.07mol%YbF₃ sample.

Figures 23 and 24 show the absorption spectra of NaF-codoped YbF₃:CaF₂ crystals in comparison with the YbF₃ doped samples; the influence of the Na⁺ ions on the absorption spectra depends on the ratio $R = y \text{ mol\%NaF} / x \text{ mol\% YbF}_3$. The absorption spectra show that the codoping with Na⁺ ions in different R ratios can modulate the spectroscopic properties of Yb³⁺ ions in CaF₂ lattice in a large scale. The differences among the spectra corresponding to ratio $R < 10$ and those $R > 15$ are distinct (see Figs. 23 and 24). The absorption spectra of the crystals with $R < 10$ and without NaF are broad and non-structured.

The absorption bands of the samples with $R > 15$ became narrower and clearly resolved into six peaks, (see Figs.23 and 24) corresponding to trigonal T₂ (Y_{T2}=910nm), cubic O_h (Y_O=922nm), trigonal T₁ (Y_{T1}=936nm), clusters sites (Y_C at 945.6 and 955nm) and trigonal C_{3v} site (Y¹=965nm) with Na⁺ ion as charge compensator. As it results from the analysis of these spectra, the presence of Na⁺ ions, at ratio $R > 20$ suppresses the peak Y_{CH}=980nm that is attributed to 1-5 transition of hexamer type clusters, and reduces also the intensity of the transitions corresponding to "small clusters", Y_C. Another effect of the Na⁺ ions is to reduce the tetragonal C_{4v} (NN) sites; for samples with $R > 20$ this site is drastically reduced, and this effect is confirmed by the dielectric relaxation measurements described in III.3.

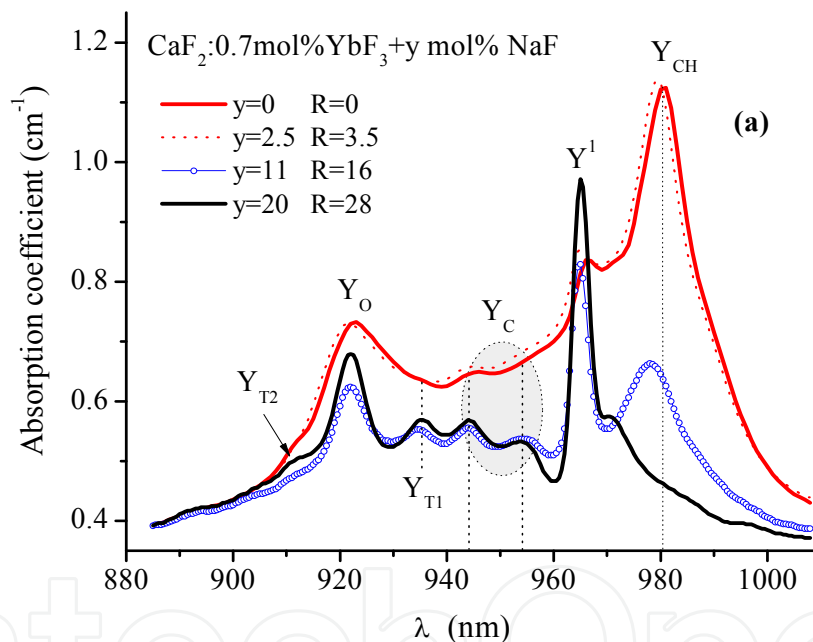


Fig. 24. Optical absorption spectra of 0.7 mol% YbF₃ doped CaF₂ crystals codoped with different amount of NaF.

The peak corresponding to hexamer cluster (Y_{CH}=980nm) is completely suppressed as well as the C_{4v} site (see Fig. 23) for the sample with $R = 36$ (0.07 mol% YbF₃ + 2.5 mol% NaF) : CaF₂. The reducing effect depends on the R ratio. Comparing the absorption spectra of Yb doped and Na⁺ ions codoped crystals it is clear that we can "tailor" the type of the compensating defects by choosing the suitable ratio R of the Na:Yb ions.

The dielectric spectra reveal two peaks that correspond to relaxation of two type of dipoles: NN (Yb³⁺- F_i centers with C_{4v} symmetry) and (Na⁺-V_F) dipoles (see III.3). The temperature and frequency dependence of ϵ_2 for Na⁺ ions co-doped samples, for ratio $R < 20$ is characterized by three peaks. For all samples the peak occurring at around 195 K at 1 kHz is associated to the R₁ (NN) center relaxation [Fontanella & Andeen, 1976; Andeen et al., 1981].

The second peak is associated to the order-disorder transition [Smolenskii et al., 1959; Nicoara, 2008] and the third peak, that appears only for Na⁺ ions codoped crystals, is associated to (Na⁺-V_F) dipoles relaxation, formed by a substitutional Na⁺ ion and a F⁻ vacancy (V_F) created to maintain the electrical neutrality of the crystal [Johnson et al., 1969; Shelley&Miller, 1970].

For heavier NaF- codoped samples, namely for ratio R>20, only one relaxation is observed, associated to the (Na⁺-V_F) dipole. This confirms the observed suppression of the peaks of optical absorption spectra, corresponding to centers with C_{4v} (NN dipole) symmetry (see the optical absorption spectra Figs. 23 and 24).

The number of dipoles N_D that contribute to the dielectric relaxation peak can be calculated from the dielectric spectra using the methods described in [Fontanella&Andeen, 1976; Campos&Ferreira, 1974].

The Na⁺- ions co-doped YbF₃:CaF₂ crystals reveal a decrease of the NN dipoles in comparison with the YbF₃- doped samples, indicating that the Na⁺ ions reduce the formation of NN type dipoles with C_{4v} symmetry; this is confirmed by the absorption spectra, see figures 23 and 24. This effect depends on the ratio R= ymol%NaF/ xmol%YbF₃, as is shown in Fig. 22a,b.; as the ratio R increases, the number of NN (C_{4v}) centers decreases and the number of (Na⁺-V_F) dipoles increases (fig.22b); for ratio R=28 and 36 no NN type relaxation was detected (fig.21b), this means a very small concentration of C_{4v} sites.

Figure 25 illustrates the variation of the (Na⁺-V_F) dipoles concentration on the YbF₃ concentration for all the studied NaF-codoped crystals, the ratio R for every sample is specified. The insert shows the dependence of the NN dipoles concentration on the NaF concentration for a given YbF₃ concentration, namely for 0.7mol% YbF₃.

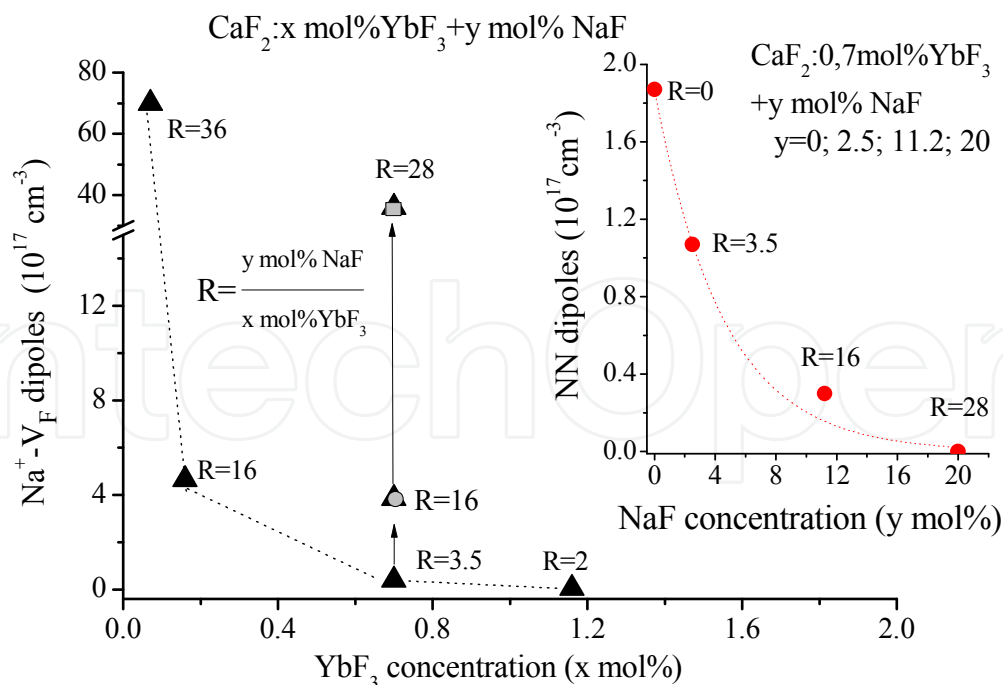


Fig. 25. Influence of YbF₃ concentration and of ratio R on the Na⁺-V_F dipoles concentration. The inset shows the influence of NaF concentration on the NN dipoles concentration for CaF₂: 0.7 mol%YbF₃ + y mol%NaF samples.

Influence of Na⁺ ions on the charge compensating defects

From the dielectric spectra results that Na⁺ ions lead to a decrease of the NN dipoles (see figs.22b and 25), the charge compensating defects with tetragonal C_{4v} symmetry and this behavior is confirmed by the absorption spectra of the samples.

Figure 26 shows the dependence on NaF concentration of the line intensity corresponding to the C_{4v} center and of the NN dipoles concentration for samples doped with 0.7 mol% YbF₃. The inset shows the dependence on the NaF concentration of the line intensity corresponding to C_{3v} site with Na⁺ ion as charge compensator, respectively of the line intensity corresponding to clusters. Taking into account that the peak intensity is proportional with the absorbant centers, we observe that as the Na⁺ ions concentration increases the charge compensating defects corresponding to C_{4v} site decrease and those corresponding to C_{3v} site increase; the decrease of the cluster type defects is also clear. The decreases of the concentration of the defects corresponding to C_{4v} site is confirmed by the decrease of the NN (C_{4v}) dipoles concentration calculated from dielectric spectra.

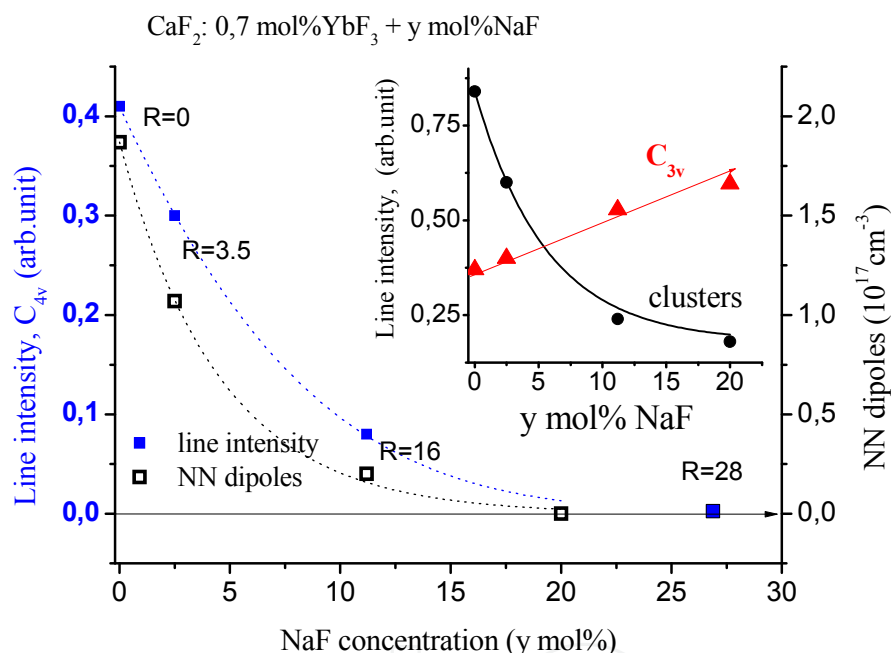


Fig. 26. Influence of NaF concentration on the line intensity of C_{4v} site and on the NN dipoles concentration. The inset shows the influence of NaF concentration on the line intensity corresponding to defects with C_{3v} symmetry with Na⁺ ion as charge compensator and on the line intensity corresponding to the clusters.

The effect of Na⁺ ions on the formation of the compensating defects can be explained this way. It is known that for concentration above about 0.05at% the rare-earth ions aggregate to form pairs, to form more or less complex centers, clusters. The most common pairs are the dimmers that consist by two Yb³⁺ ions and two F_i⁻ ions and the hexameric clusters [Petit et al., 2008]. The Na⁺ ions substitute one of the partners of the pairs and lead to an increased number of pseudo-isolated centers, like C_{3v} site with Na⁺ ion as charge compensator, without dipolar properties. This pair-breaking effect is more effective on the hexameric clusters than on the smaller clusters; for R= 28 and 36 the optical absorption peak (at 980nm) associated to hexamer clusters is suppressed, as is also illustrated in figures 23 and 24. As results from our investigation, codoping with Na⁺ the YbF₃ doped CaF₂ crystals it

is possible to “tailor” the type of the compensating defects by choosing the suitable ratio R of the Na:Yb ions.

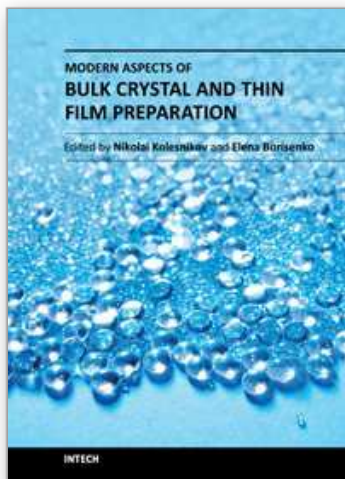
The experimental results showed that codoping with Na⁺ ions in different Na:Yb ratios we can modulate the spectroscopic properties of Yb³⁺ ions in CaF₂ host. The influence of Na⁺ ions on the defects formation is discussed taking into account the optical absorption spectra and the calculated number of NN dipoles whose relaxation are observed. By choosing the suitable ratio of the Na:Yb ions it is possible to “tailor” the type of the compensating defects in YbF₃ doped CaF₂ crystals.

4. References

- Andeen, C.; Link, D. & Fontanella, J. (1977). Cluster-associated relaxations in rare-earth-doped calcium fluoride. *Phys Rev. B*, Vol. 16, pp. 3762-3767
- Andeen, C.; Matthews, G. E.; Smith, M.K. & Fontanella, J. (1979). Electric dipole relaxation of mixed clusters in double-doped CaF₂. *Phys. Rev. B*, Vol. 19, pp. 5293-5298
- Barat, C. (1995), Origines thermiques et convectives des segregations solutales dans des alliages semiconducteurs. PhD. Thesis, University of Rennes
- Barraldi, A.; Capelletti, R.; Mazzera, M.; Ponzoni, A.; Amoretti, G.; Magnani, N.; Toncelli, A. & Tonelli, M. (2005). Role of Er³⁺ concentration in high-resolution spectra of BaY₂F₈ single crystals. *Phy. Rev. B*, Vol. 72, pp. 075132
- Benson, K.K. & Dempsey, E. (1962). The cohesive and surface energies of some crystals possessing the fluorite structure. *Proc. Roy. Soc. Lond. A*, Vol. 366, pp. 344-358
- Bridgman, P.W. (1925). Crystal growth apparatus. *Proc. Am. Acad. Arts Sci.*, Vol. 60, pp. 305
- Campos, V.B. & Leal Ferreira, G.F. (1974). Dipolar studies in CaF₂ with Ce³⁺. *J. Phys. Chem. Solids*, Vol. 35, pp. 905-910
- Chang, C.E. & Wilcox, W.R. (1974). Control of interface shape in the vertical bridgman-stockbarger technique. *J. Cryst. Growth*, Vol. 21, pp. 135-140
- Corish, J.; Catlow, C.R.A.; Jacobs, P.W.M. & Ong, S.H. (1982). Defect aggregation in anion-excess fluorites. Dopant monomers and dimers. *Phys. Rev. B*, Vol. 25, pp. 6425
- Doualan, J.L.; Comy, P.; Brnayad, A.; Minard, V.; Moncorge, R.; Boudeile, J.; Druon, F.; Georges, P. (2010), Yb³⁺ doped (Ca,Sr,Ba)F₂ for high power laser applications, In: *Laser Physics*, Pashemin, P., pp.533-537, Springer Publishing, ISSN 1054-660X
- Feofilov, P.P. (1956). Absorption and luminescence of divalent rare-earth ions in fluoride crystals. *Opt. Spectrosc.*, Vol. 1, pp. 992-1000
- Fong, F.K. (1964). Electrolytic reduction of trivalent rare-earth ions in alkalin-earth halides. *J. Chem. Phys.*, Vol. 41, pp. 2291-2296
- Fontanella, J. & Andeen, C. (1976). The dielectric spectrum of erbium doped CaF₂. *J. Phys. C*, Vol. 9, pp. 1055
- Fontanella, J. & Treacy, D.J. (1980). The effect of quenching on the defect structure of calcium fluoride doped with erbium. *J. Chem. Phys.*, Vol. 72, pp. 2235-2244
- Fontanella, J.; Chadwick, A.V.; Carr, V.M.; Wintersgill, M.C. & Andeen, C.G. (1980). Dielectric relaxation studies of alkali-metal-doped calcium fluoride. *J. Phys. C: Solid State Phys.*, Vol. 13, pp. 3457-3466
- Fu, T.W. & Wilcox, W.T. (1980). Influence of insulation on stability of interface shape and position in the vertical Bridgman-Stockbarger technique. *J. Cryst. Growth*, Vol. 48, pp. 416-424

- Gault, W.A.; Monberg, E.M. & Clemans, J.E. (1986). A novel application of the vertical gradient freeze method to the growth of high quality III-V crystals. *J. Cryst. Growth*, Vol. 74, pp. 491-506
- Hurle, D.T.J. (1993), Crystal pulling from the melt, Springer-Verlag, Berlin, ISBN 3540566767
- Jasinski, T.; Rohsenow, W.M. & Witt, A.F. (1983). Heat transfer analysis of the Bridgman-Stockbarger configuration for crystal growth: I. Analytical treatment of the axial temperature profile. *J. Cryst. Growth*, Vol. 61, pp. 339-354
- Johnson, H.B.; Tolar, N.J.; Miller, G.R. & Cutler, I.B. (1969). Electrical and mechanical relaxation in CaF₂ doped with NaF. *J. Phys. Chem. Solids*, Vol. 30, pp. 31-42
- Kaczmarek, S.M.; Tsuboi, T.; Ito, M.; Boulon, G. & Leniec, G. (2005). Optical study of Yb³⁺/Yb²⁺ conversion in CaF₂ crystals. *J. Phys.:Condens. Mater.*, Vol. 17, pp. 3771-3786
- Kaplyanskii, A.A. & Feofilov, P.P. (1962). Absorption spectra of divalent rare-earth ions in fluoride crystals. *Opt. Spectrosc.*, Vol. 13, pp. 235-241
- Kaplyanskii, A.A. & Smolyanskii, P.L. (1976), Effect of external fields on optical absorption spectra of SrCl₂ : Yb²⁺. *Opt. Spectrosc.*, Vol. 40, pp. 528-540
- Kirton, J. & McLaughlan, S.D. (1967). Correlation of electron paramagnetic resonance and optical absorption spectra of CaF₂:Yb³⁺. *Phys. Rev.*, Vol. 155, pp. 279-284
- Kuwano, Y. (1982). Effective distribution coefficient of neodymium in Nd:Gd₃Ga₅O₁₂ crystals grown by the Czochralski method. *J. Crystal Growth*, Vol. 57, pp. 353-361
- Lifante, G.; Cantelar, E.; Munoz, J.A.; Nevado, R.; Sanz-Garcia, J.A. & Cusso, F. (1999). Zn-diffused LiNbO₃:Er³⁺/Yb³⁺ as a waveguide laser material. *Opt. Mat.*, Vol. 13, pp. 181-186
- Mikkelsen, I.C. Jr. (1980). Three-zone Bridgman-Stockbarger crystal growth furnace. *Rev. Sci. Instrum.*, Vol.51, pp. 1564-1566
- Mitric, A.; Duffar, T.; Diaz-Guerra, C.; Corregidor, V.; Alves, L.C.; Garnier, C. & Vian, C. (2006). Growth of Ga_(1-x)In_xSb alloys by Vertical Bridgman technique under alternating magnetic field. *J. Cryst. Growth*, Vol. 287, pp. 224-229
- Naumann, R.I. (1982). An analytical approach to thermal modeling of Bridgman-type crystal growth : I. One-dimensional analysis. *J. Cryst. Growth*, Vol. 58, pp. 554-568
- Nicoara, D. (1975). Metal single crystals growth set-up. Romanian Patent nr.62842
- Nicoara, D.; Schlett, Z. & Nicoara, I. (1983). Optical crystals growth set-up. Romanian Patent nr. 82663
- Nicoara, D. & Nicoara, I. (1984). Crucibles for optical crystals growth. Romanian Patent nr. 85993
- Nicoara, D.; Nicoara, I. & Schlett, Z. (1985). Heater for large diameter crystals growth. Romanian Patent nr. 88497
- Nicoara, I.; Aczel, O.F.G.; Nicoara, D. & Schlett, Z. (1986). Dissolution kinetics and etch pit morphology of CaF₂ single crystals. *Crys. Res. Technol.*, Vol. 21, pp. 647-652
- Nicoara, I.; Nicoara, D. & Aczel, O.F.G. (1987). Crystal growth in an improved bridgman variable shape graphite furnace. *Crys. Res. Technol.*, Vol. 22, pp. 1139-1144
- Nicoara, D. & Nicoara, I. (1988). An improved Bridgman-Stockbarger crystal-growth system. *Mat. Science and Engineering A*, Vol. 102, L1-L4
- Nicoara, I; Munteanu, M.; Pecingina-Garjoaba, N.; Stef, M. & Lighezan, L. (2006a). Dielectric spectrum of rare-earth-doped calcium fluoride crystals. *J. Crystal Growth*, Vol. 287, pp. 234-238

- Nicoara, I.; Munteanu, M.; Pecingina-Garjoaba, N.; Stef, M. & Lighezan, L. (2006b). Dielectric relaxation in PbF₂-doped and X-ray irradiated CaF₂ crystals. *ECS Transactions*, Vol. 3, pp. 51-58
- Nicoara, I.; Pecingina-Garjoaba, N. & BunoIU, O. (2008a). *J. Crystal Growth*, Vol. 310, pp. 1476-1480
- Nicoara, I.; Lighezan, L.; Enculescu, M. & Enculescu, I. (2008b). Optical spectroscopy of Yb²⁺ ions in YbF₃-doped CaF₂ crystals. *J. Crystal Growth*, Vol. 310, pp. 2026-2032
- Nicoara, I.; Stef, M. & Pruna, A. (2008c). Growth of YbF₃-doped CaF₂ crystals and characterization of Yb³⁺/Yb²⁺ conversion. *J. Crystal Growth*, Vol. 310, pp. 1470-1475
- Nicoara, I.; Munteanu, M.; Preda, E. & Stef, M. (2008d). Some dielectric and optical properties of ErF₃-doped CaF₂ crystals. *J. Crystal Growth*, Vol. 310, pp. 2020-2025
- O'Connor, J.R. & Bostick, H.A. (1962). Radiation effects in CaF₂:Sm. *J. Appl. Phys.*, Vol. 33, pp. 1868-1870
- Paraschiva, M.; Nicoara, I.; Stef, M. & BunoIU, M. (2010). Distribution of Pb²⁺ ions in PbF₂-doped CaF₂ crystals. *Acta Physica Polonica A*, Vol. 117, pp. 466-470
- Petit, V.; Camy, P.; Doualan, J.L. & Moncorge, R. (2007). Refined analysis of the luminescent centers in the Yb³⁺:CaF₂ laser crystal. *J. of Luminesc.*, Vol. 122-123, pp. 5-7
- Petit, V.; Camy, P.; Doualan, J.L.; Portier, J. & Moncorge, R. (2008). Spectroscopy of Yb³⁺:CaF₂: From isolated centers to clusters. *Phys. Rev. B*, Vol. 78, pp. 085131
- Pruna, A.; Stef, M. & Nicoara, I. (2009). Dielectric spectra of Li⁺ (Na⁺) codoped CaF₂:YbF₃ crystals. *Phys. Stat. Sol. A*, Vol. 206, pp. 738-744
- Sangwal, K. & Arora, S.K. (1978). Etching of MgO crystals in acids: kinetics and mechanism of dissolution. *J. Mater. Sci.*, Vol. 13, pp. 1977-1985
- Shelley, R.D. & Miller, G.R. (1970). Ionic thermocurrent study of the dipole-dipole interaction in CaF₂ doped with NaF. *J. Solis State Chemistry*, Vol. 1, pp. 218-226
- Stockbarger, D.C. (1949). Artificial fluorite. *J. Opt. Soc. Am.*, Vol. 39, pp. 731-740
- Strukov, B.A. & Levanyuk, A.P. (1998), *Ferroelectric Phenomena in crystals*, Springer, Berlin, ISBN 3540631321
- Su, L.; Xu, J.; Li, H.; Wei, L.; Yang, W.; Zhao, Z.; Si, J.; Dong, Y. & Zhou, G. (2005). Crystal growth and spectroscopic characterization of Yb-doped and Yb, Na-codoped CaF₂ laser crystals by TGT. *J. Crystal Growth*, Vol. 277, pp. 264-268
- Su, L. & all. (2005). Sites structure and spectroscopic properties of Yb-doped and Yb, Na-codoped CaF₂ laser crystals. *Chem. Phys. Lett.*, Vol. 406, pp. 254-258
- Su, L. & all. (2007). Quaternary doping to improve 1.5 μm quantum efficiency of Er³⁺ in CaF₂ single crystal. *J. of Luminesc.*, Vol. 122-123, pp. 17-20
- Sun, D.; Zhang, Q.; Wang, Z.; Su, J.; Go, C.; Wang, A. & Yin, S. (2005). Concentration distribution of Nd³⁺ in Nd:Gd₃Ga₅O₁₂ crystals studied by optical absorption method. *Cryst. Res. Technol.*, Vol. 40, pp. 698-702
- Yonezawa, T.; Nakayama, J.; Tsukuma, K. & Kawamoto, Y. (2002). Behaviors of trace amounts of metal-oxide impurities in CaF₂ crystal grown by Stockbarger's method. *J. Cryst. Growth*, Vol. 244, pp. 63-69



Modern Aspects of Bulk Crystal and Thin Film Preparation

Edited by Dr. Nikolai Kolesnikov

ISBN 978-953-307-610-2

Hard cover, 608 pages

Publisher InTech

Published online 13, January, 2012

Published in print edition January, 2012

In modern research and development, materials manufacturing crystal growth is known as a way to solve a wide range of technological tasks in the fabrication of materials with preset properties. This book allows a reader to gain insight into selected aspects of the field, including growth of bulk inorganic crystals, preparation of thin films, low-dimensional structures, crystallization of proteins, and other organic compounds.

How to reference

In order to correctly reference this scholarly work, feel free to copy and paste the following:

Irina Nicoara and Marius Stef (2012). Growth and Characterization of Doped CaF₂ Crystals, Modern Aspects of Bulk Crystal and Thin Film Preparation, Dr. Nikolai Kolesnikov (Ed.), ISBN: 978-953-307-610-2, InTech, Available from: <http://www.intechopen.com/books/modern-aspects-of-bulk-crystal-and-thin-film-preparation/growth-and-characterization-of-doped-caf2-crystals>

INTECH
open science | open minds

InTech Europe

University Campus STeP Ri
Slavka Krautzeka 83/A
51000 Rijeka, Croatia
Phone: +385 (51) 770 447
Fax: +385 (51) 686 166
www.intechopen.com

InTech China

Unit 405, Office Block, Hotel Equatorial Shanghai
No.65, Yan An Road (West), Shanghai, 200040, China
中国上海市延安西路65号上海国际贵都大饭店办公楼405单元
Phone: +86-21-62489820
Fax: +86-21-62489821

© 2012 The Author(s). Licensee IntechOpen. This is an open access article distributed under the terms of the [Creative Commons Attribution 3.0 License](#), which permits unrestricted use, distribution, and reproduction in any medium, provided the original work is properly cited.

IntechOpen

IntechOpen